ADDITIVE MANUFACTURE OF ADVANCED COMPOSITES USING REACTIVE RESINS AND CONTINUOUS CARBON FIBER

A Thesis
Submitted to the Graduate Faculty
of the
North Dakota State University
of Agriculture and Applied Science

By

Bibek Aryal

In Partial Fulfillment of the Requirements
for the Degree of
MASTER OF SCIENCE

Major Department:
Mechanical Engineering

December 2023

Fargo, North Dakota

North Dakota State University
Graduate School

Title

ADDITIVE MANUFACTURE OF ADVANCED COMPOSITES USING REACTIVE RESINS AND CONTINUOUS CARBON FIBER

By

Bibek Aryal

The Supervisory Committee certifies that this ***disquisition*** complies with North Dakota State University's regulations and meets the accepted standards for the degree of

MASTER OF SCIENCE

SUPERVISORY COMMITTEE:

Dr. Chad Ulven
Chair

Dr. Long Jiang

Dr. Dean Webster

Approved:

February 26, 2024 — Date

Dr. Chad Ulven — Department Chair

ABSTRACT

To overcome the significant limitations such as slow processing times, substantial energy needs of conventional additive manufacturing technology, reactive extrusion additive manufacturing (REAM) process was developed. As printed objects with neat reactive resin exhibited insufficient mechanical performance for advanced application, continuous fiber reinforcement is an effective route to improve mechanical performances. Continuous carbon fiber reinforced 3D printing was performed using a commercially available reactive resin system and an experimentally synthesized one at NDSU. The mechanical properties of the printed carbon fiber reinforced samples were compared with the neat resin samples. The tensile strength of printed sample using Pentaerythritol-xylendiamine resin system increased by 217% with 2.88% carbon fiber content. Similarly tensile strength of Epon-Epikure sample increased by 151% with the fiber-volume fraction of 4.4%. Therefore, reinforcement with continuous carbon fiber has potential to overcome the barrier of low mechanical strength exhibited by neat reactive resin system.

ACKNOWLEDGMENTS

First of all, I would like to thank Army Research Laboratory for funding this research project. I would like to thank my advisor Dr. Chad Ulven for providing me continuous guidance and leadership throughout this research. I would like to acknowledge Luke Gibbon and Eric Hall for their continuous immense support and guidance throughout this project. I would also like to acknowledge my committee members Dr. Long Jiang and Dr. Dean Webster for providing me guidance throughout this study. I would like to thank my lab mates who helped me during this project.

Finally, I would like to thank my friends and family who supported me.

DEDICATION

I would like to dedicate this thesis to my parents and family.

TABLE OF CONTENTS

LIST OF TABLES

LIST OF FIGURES

LIST OF ABBREVIATIONS

AM .....Additive Manufacturing.

PX .....Pentaerythritol and m-xylylenediamine.

3D.....Three dimensional.

SLA .....Stereolithography.

CAD .....Computer aided design.

FDM.....Fused deposition modeling.

DLP .....Digital light processing.

UV.....Ultraviolet.

REAM.....Reactive extrusion additive manufacturing.

CFRP.....Carbon fiber reinforced polymer.

FRPC.....Fiber reinforced polymer composite.

LIST OF SYMBOLS

D ..... Density of polymer/composite.

a ..... Dry mass of the polymer/composite.

b_1 ..... Apparent mass of the fully immersed polymer

ρ ..... Density of water.

E ..... Modulus of elasticity.

σ_T ..... Tensile stress.

ε_T ..... Tensile strain.

P ..... Load.

L ..... Support span length.

b ..... Width of beam.

d ..... Depth of beam.

σ_f ..... Flexural stress.

σffn ..... Flexural stress at predefined point

$\varepsilon\varepsilon ffn$ ..... Flexural strain at predefined point.

V_f ..... Fiber volume fraction.

m_f ..... Mass of fiber.

ρ_f ..... Density of fiber.

ρ_m ..... Density of matrix.

M_m ..... Mass of matrix.

E_c ..... Modulus of composite.

E_m ..... Modulus of matrix.

σ_c ..... Stress of composite.

σ_m ..... Stress of matrix.

1. INTRODUCTION

Additive manufacturing (AM), commonly known as three-dimensional (3D) printing, is a production process which can create complex and specialized parts. This technology, offering considerable flexibility over conventional manufacturing processes, has been gaining popularity across various industries [1]. As per the market analysis report from Grand View Research (San Francisco, CA), the worldwide market for 3D printing reached a valuation of USD 16.75 billion in 2022 [2]. The report anticipates an annual growth rate of 23.3% from 2023 to 2030 in the market size. AM is a layer-by-layer process of manufacturing objects from three-dimensional models. This manufacturing process produces objects by adding materials until the required geometrical shape is achieved [3]. The process starts with a meshed 3D computer model, which is designed by computer aided design (CAD) software. The meshed design is then sliced into a build file and sent to the printer to create desired object. AM can encompass metals, polymers, and ceramics; nevertheless, the scope of this investigation is centered around polymer AM. AM was first commercially used in 1987 in the form of stereolithography (SLA) [4]. Due to its adaptability and affordability for use in rapid prototyping and manufacturing applications, AM has grown exponentially in recent years. Over the past two decades, a variety of unique AM processes have been created with applications in aerospace, automotive, biomedical, digital art, architectural design, etc. [5]. Due to its advantages, various AM techniques are in high demand across a wide range of industries [6]. AM has several advantages over traditional manufacturing techniques, the ability to manufacture complex objects such as honeycomb structures [3],[4],[6]. However, the AM industry is working to overcome issues such as weak interlaminar adhesion and a limited selection of 3D printable materials [7].

There are numerous AM techniques available today such as SLA, digital light processing (DLP), fused deposition modeling (FDM), reactive extrusion additive manufacturing (REAM). Among them, most commonly used and popular ones are SLA and fused deposition modeling (FDM) [8]. Although the materials and production methods used in different AM technologies can differ, the basic principle of layer-by-layer manufacturing is the same. Stratasys (Eden Prairie, MN) developed FDM in the late 1980's [9]. FDM gained popularity as a result of its affordability and versatility in terms of material utilization. In the FDM technique, thermoplastic material, in the form of filament is fed through a heated extrusion nozzle [10]. The movement of the heated extrusion nozzle head is controlled by a 3-axis system that moves in the x-y plane in accordance with the software's tool path and deposits the first layer [11]. After completing one layer, the head moves in the z-direction by the amount specified for layer thickness [11]. The material deposition occurs in successive layers until the entire part is completed [10], [11]. Parts manufactured with thermoplastic materials are more versatile due to their ability to be reshaped and recycled [12]. On the other hand, AM thermoset parts offer high strength and resilience, hence are ideal for applications in industries such as automobile and aerospace that require high temperature stability and chemical resistance [13].

SLA and DLP are among the AM processes that use thermoset resins. The process of SLA involves successively printing thin layers of a curable substance, such as ultraviolet (UV)-curable material, one on top of the other to create solid objects. To form a solid cross-section of the object at the liquid's surface, a programmed movable spot beam of UV light shining on a surface or layer of UV-curable liquid is used [9]. A UV laser is directed in a specific direction to shoot in the resin, and the photocurable resin polymerizes into a patterned layer [14]. The first layer is cured, and another layer is deposited on the previous layer. This process continues until the final layer of the

desired shape is created. In some cases, thermal curing is also achieved by using a high-energy laser [15]. Post-processing of high-frequency wavelength is required for UV curable resins to achieve the desired shape. The working principle of DLP is similar to the SLA process. DLP uses projector light whereas SLA uses fast moving laser light for curing.

REAM or reactive resin 3D printing process follows the material extrusion-based principle with the utilization of two-part reactive thermoset resin system. The metering system extracts two precursors -thermoset resin and hardening agent from separate reservoirs and pumps them in a reactive extrusion process. In this method, a multi-part thermoset resin is mixed with a hardening (catalyst) agent just before the extrusion process, resulting in the formation of 3D objects [14], [16].

1.1. Reactive Resin

Reactive resins undergo solidification often via chemical reactions which is triggered with the help of curing agent or catalyst. The chemical reaction involves the cross linking of polymers chain. The most common reactive resin used has three classifications, namely epoxy-based resins, polyurethanes, and polyesters.

Among these, epoxy resins are widely used due to their diverse curing systems, including heat curing, photo curing and room-temperature curing using amines or diacid compounds as a curing agent. Epoxy functional resins is the resin system, where epoxy sides are made from an oligomer containing at least two epoxide groups that are crosslinked with a hardening or curing agent [17]. These resins find applications in various fields, including coatings, aerospace, biomedical, and electronics industries [18].

Polyurethanes are formed by simultaneously mixing isocyanate and polyol molecules, each having multiple isocyanate groups (R–(N=C=O) $n \geq 2$) and hydroxyl groups (R'–(OH)$n \geq 2$) in

the presence of a catalyst or UV light. Typically, properties of polyurethanes depend upon the type of polyols and isocyanates. Polymeric materials manufactured from polyurethanes are dependent on the amount of crosslinking. Polyurethanes are also widely applicable in the field of automotive (manufacturing seats, car bodies, bumpers, and various other components of vehicles), marine, the coating industry, medical industry, appliances, and flooring where their versatility is a valuable asset [19].

Epoxy resins are generally more suitable for high-temperature applications, as they offer excellent heat resistance and the ability to withstand elevated temperatures without compromising their properties. Epoxy resin in the combination of hardening agent is used in this study.

1.2. AM using Reactive Resin

The two-part reactive AM system utilizes the principle of mixing both components within the mixing chamber before deposition on the print bed. Those components undergoes a fast-cross-linking reaction to create desired object [16], [17], [20]. This system uses a layer-by-layer process to print the required geometry. This system utilizes a dual pump system to pump each component to the mixing chamber and dispense the mixed resin through a nozzle. The ratio of mixing both liquid components together is controlled with the driving mechanism. Complete curing of the resin would not happen if the ratio of the component is not controlled properly. Thus, uncured resins may spread on the printing bed.

Mixing two-part reactive resins is one of the most crucial factors in two-part reactive resin AM system. In particular, proper mixing of two-part polyurethane or polyurea is vital. Proper mixing plays an important role in the 3D printing using reactive resins. If the mixing is insufficient, the resin will not be able to fully cure and reduce the properties of the printed samples. Inhomogeneous mixing can lead to weak spots or defects in the printed samples, reducing its

performance. Effective mixing needs to be accomplished in order to encompass a reinforcing fiber with a matrix which exhibits good bonding, increasing strength, stiffness, and other mechanical properties. Additionally, effective mixing can also lead to reduce material wastage, production costs and the number of raw materials required to achieve the desired properties of the printed samples [21], [22].

Mixing can be performed in numerous ways like dynamic, static and impingement mixing. Dynamic mixing involves the use of mechanical agitators, mixers, or impellers to create turbulence and promote the mixing of materials in a vessel or container [23]. Impingement mixing, also known as collision or jet mixing, where the mixing occurs as two high-velocity streams collide with sufficient force in a mixing chamber. The cost of this type of mixing can be high as it requires high velocity. Static mixing is mostly used for continuous mixing processes [21]. Compared to all other mixing methods, static mixing has better properties in terms of cost, flow, and cure. Unlike other approaches, static mixing does not rely on high fluid velocity. Instead, it employs a design comprising mixing elements arranged at a 90° offset from one another. This offset interrupts the fluids' path, prompting both fluids to fold into each other until they achieve a uniform and homogeneous mixture [21].

Uitz *et al*. conducted the study on AM of isotropic parts using a two-part reactive system, static mixing nozzle, and dual pump system. They demonstrated the REAM using reactive resin system. They used Epon 8111 as epoxy resin and Epikure 3271 as curing agent to manufacture composites via REAM [16], [24]. In their study they manufactured parts with 48 mm height and analyzed the thermal characteristics during the printing process and isotropic properties of the printed specimen. Exothermic reaction was observed after mixing. It has been concluded that the REAM parts can be manufactured significantly faster than conventional AM systems where the

volumetric deposition rate was found almost 20 times higher than FDM process produced by Jamison Go and A. John heart of MIT [16].These REAM parts surpassed ABS, PLA and nylon components in tensile strength and stiffness, eliminating need for energy-intensive material processing during printing and post-printing anisotropy corrections. This finding offers a promising avenue for large-scale AM with unparalleled deposition rates [16]. Romberg *et al*. successfully conducted the large-scale additive manufacturing using two-part reactive resin system. They characterized the effects of heat generation and crosslinking during the printing process in a large-scale AM process with the help of infrared and optical vision systems[25]. There has been several studies on AM with reactive resins [16], [24], [25]. However, the printed objects possess insufficient stiffness and strength required for high performance applications [16]. To further improve the mechanical properties, fiber reinforcement can be introduced with reactive resin to 3D print composites. Carbon fiber reinforced polymers (CFRPs) find widespread use in the automotive, aviation, and wind energy industries, where the emphasis on weight reduction is crucial. These advanced materials boast high specific toughness, significant specific rigidity, low weight, and excellent corrosion resistance [26]–[28].

1.3. AM with Continuous Carbon Fiber

Several studies have been done on AM of composites using thermoplastic and thermosetting resins with continuous carbon fiber reinforcement. Some research on AM of thermoplastic and thermoset resin reinforced with continuous carbon fiber has been performed following the principle of FDM based extrusion printing process and “Direct ink write based printing process”, respectively.

Hirano *et al.* conducted a study on 3D printing of continuous carbon fiber reinforced composites using PLA as a thermoplastic matrix material. They used in-situ impregnation of carbon

fiber and matrix material. Matrix material was melted using a heated-extruder and mixed with continuous carbon fiber within the nozzle. The fiber-volume fraction of printed CCF reinforced composites was found 6.6% [29]. Moreover, MarkForged (Waltham, MA) commercialized the 3D printer which can print continuous carbon fiber coated with thermoplastic matrix material in 2014. It utilizes continuous carbon, glass and aramid fiber prepreged with nylon filament [30], [31].

Hao *et al*. performed a study on 3D printing of continuous carbon fiber reinforced composites using Direct ink write based printing process. They utilized epoxy resin as a thermosetting material and 3k tow carbon fiber as a reinforcement. It was found that the tensile strength and modulus of the printed composite were 792.8 MPa and 161.4 GPa respectively. Similarly, the flexural strength and modulus were determined to be 202 MPa and 143.9 GPa respectively [32]. The authors claimed that the resulting mechanical properties of the printed composites were better than similar printed thermoplastic composites.

Ming et. al. optimized the process parameters of 3D printed continuous carbon fiber reinforced thermoset composites that utilized direct ink write based printing process. The maximum flexural strength and modulus of the 3D printed sample with 58 weight% carbon fiber content were found to be 952.89 MPa and 74.05 GPa respectively [33]. The optimized materials and process significantly increased the mechanical properties.

Moreover, AM with continuous carbon fiber and thermoset resin was demonstrated using UV-light and thermic-lance assisted printing process. Dong et.al. conducted the study on continuous carbon fiber reinforced thermosetting composites using thermic-lance assistance. They found the flexural strength and modulus of printed sample as 471.1 MPa and 41.1 GPa [34].

Based on authors knowledge, no literature is available on 3D printing of continuous carbon fiber reinforced composites with reactive resin system. Hence, this research is primarily focuses

on creating continuous carbon fiber reinforced polymer composites using two-part reactive resin systems. In this study, continuous fiber reinforced composites were 3D printed using two different reactive resin systems to identify the improvement in mechanical strength due to continuous carbon fiber reinforcement. To accomplish this objective, this study compares the mechanical performances of carbon fiber reinforced 3D printed composites sample with the printed sample using neat reactive resins. The hypothesis of this study is that the mechanical performance of the 3D printed carbon reinforced composites will exhibit significant improvement compared to 3D printed composites comprising only the neat reactive resin system. These improvements may broaden the potential use of 3D printed carbon reinforced composites in aerospace, defense, and automotive applications.

2. OBJECTIVES

The primary objective of this research is to print continuous carbon fiber reinforced composite with reactive resin system. This research uses two different reactive resin system to evaluate their printing and mechanical performances with continuous carbon fiber reinforcement. Hence, a commercial reactive resin system and resin system developed by NDSU polymers and coatings department was used to 3D print with continuous carbon fiber reinforcement. The overall goal of this research is to compare the improvement in mechanical properties of the printed composites due to continuous carbon fiber reinforcement. For this purpose, mechanical properties of composite 3D printed with and without carbon fiber reinforcement were compared.

To accomplish this objective following task were carried out,

- Developed a printer system that can print composites using reactive resins and continuous carbon fiber.
- Built a system to homogeneously mix two components together in a proper ratio.
- Designed a nozzle that allows feeding the carbon fiber continuously without the resin backflow and clogging issue.
- Printed continuous carbon fiber composites.
- Characterized different 3D printed specimens.

3. MATERIAL

First reactive resin used in this study comprises of epoxy resin, Epon 8111 and curing agent Epikure 3271. These were commercially available through West Lake Epoxy. This resin system was selected because of its printability using REAM process [24]. Tables 1 and 2 show the properties of the epoxy resin, Epon 8111 and Epikure 3271 curing agent. The mixing ratio used for this resin system is 4:1.

Table 1: Properties of Epon 8111 Resin [35].

Property	**Value**	**Test method**
Viscocity@25 ºC	800-1100 cp	ASTM D445
Weight/epoxide	300-320 g/eq	ASTM D1652
Density@25 ºC	1.14 g/cm^3	

Table 2: Properties of Curing Agent Epikure 3271 [36].

Property	**Value**	**Test method**
Viscocity@25 ºC	100-200 cp	ASTM D2196
Density@25 ºC	1.01 g/cm^3	ASTM D1475

The second resin used in this study was Pentaerythritol m-Xylendiamine (PX) resin system developed by Polymer and Coatings Department, NDSU. PX resin system is a resin system that comprises of acetoacetate group pentaerythritol with m-xylendiamine as an amine. The mixing ratio used for this system was 2.3:1. The glass transition temperature for PX resin system was found at 124 °C from DSC test. The maximum exothermic temperature reached during the ideal curing of this resin system was 69.2 °C.

Commercially available Toray T300-3K-40A carbon fiber is used for this research. This carbon fiber consists of 3000 individual filaments, which is also called 3K tow. It features 22-28 S-twists, or left-handed twists, per meter of fiber. The mechanical properties of T300 carbon fiber

is shown in Table 3. According to the manufacturers data sheet, the failure strain of carbon fiber was found at 1.5% with tensile strength of 3530 MPa.

Table 3: Mechanical Properties of Carbon Fiber T300 [37].

Fiber Type	**Tensile strength**	**Tensile modulus**	**Failure strain**	**Common Applications**
T300	3530 MPa	230 GPa	1.5%	Various including weaving and prepreg, especially for drapability

4. METHODS AND EQUIPMENT

4.1. Printing Principle

The schematic of the printing system is represented in Figure 1. Two separate reservoirs were used for storing the resin and hardening agent. Two separate flow channels for each part were used to dispense the fluids from the reservoir. This system draws thermoset resins and hardeners from separate reservoirs and pumps them in a defined appropriate ratio into the mixing chamber/nozzle, where the exothermic reaction begins. The resin and hardening agent were mixed in proper mixing ratio. The venturi nozzle was attached to the static mixing nozzle, where the carbon fiber was fed continuously. As a result, the mixed thermoset resins along with carbon fiber were extruded through nozzle. The fiber was bonded with matrix on the print bed. Desired composite was printed by using a layer by layer process as shown in figure below (Figure 1).

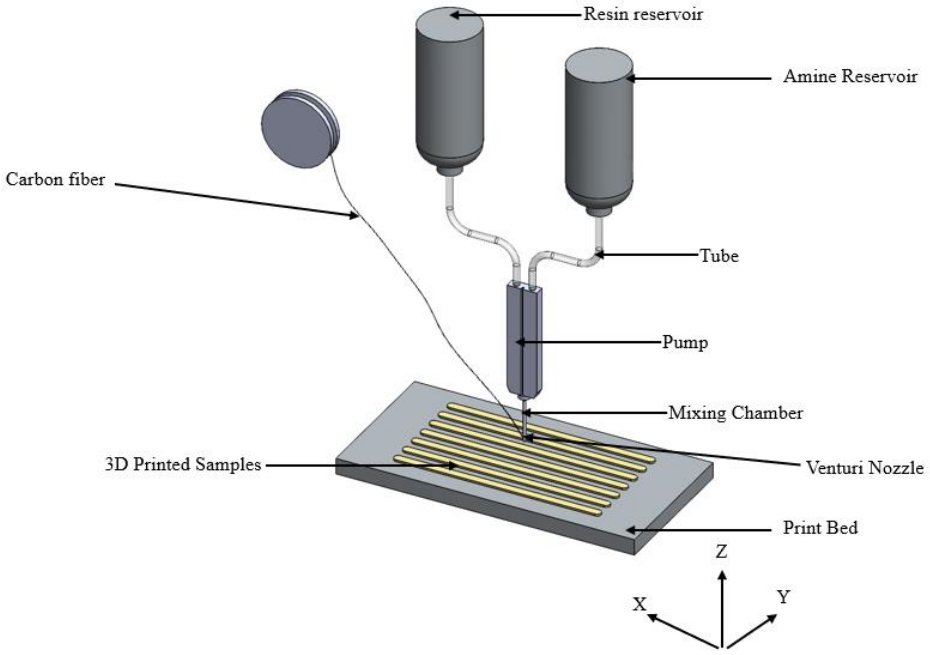

Figure 1: Schematic of printing system.

4.2. Design of Printing System

Initially, ADIMLab Gantry Pro FDM printer, purchased from ADIMLab (Shenzhen, China) was modified by Dallas Patton at North Dakota State University to print the composites using reactive resins and carbon fiber as shown in Figure 2 (a). Print bed dimensions of this printer were 300 X 300 mm with the maximum print speed of 150 mm/s. Following the prior work done by Dallas Patton, two syringe driver pumps were used separately to dispense the fluid from each syringe as shown in Figure 2 (b). The syringes were used as a reservoir for the amines and resins. Thus, drawn thermoset resins were mixed in the helical static mixer which was printed in SLA printer as shown on Figure 2 (c). An SLA 3D printed static mixer was used inside an aluminum pipe which functioned as mixing chamber that consisted of two threaded brass tube fittings and a stainless-steel wye-connector. In Patton's research plastic tubes were connected from syringes to tube fittings. The venturi nozzle that also had the fiber inlet hole was attached at the end of mixing chamber using tubes and fittings that allowed consistent and laminar flow.

Due to dimensional inaccuracy of printed mixers, resins would slide down the walls of the tube and push out the static mixer. It was found that mixing of the resins was not sufficient. The system was unable to print anything beyond the ratio of 2:1. The syringe pumps used were not able to effectively dispense the two components in the mixing chamber. Moreover, the cleaning of mixing chamber was required after each print which was time consuming. Debris were observed in the mix chamber which unnecessarily reacted with the resins during the print. Backflow of resins was also observed. Finally, the system was not able to print the composites effectively at a large scale. To address these issues and print composite with high resolution, a new printing system was developed using ShopBot (ShopBot Tools, Durham,NC) gantry.

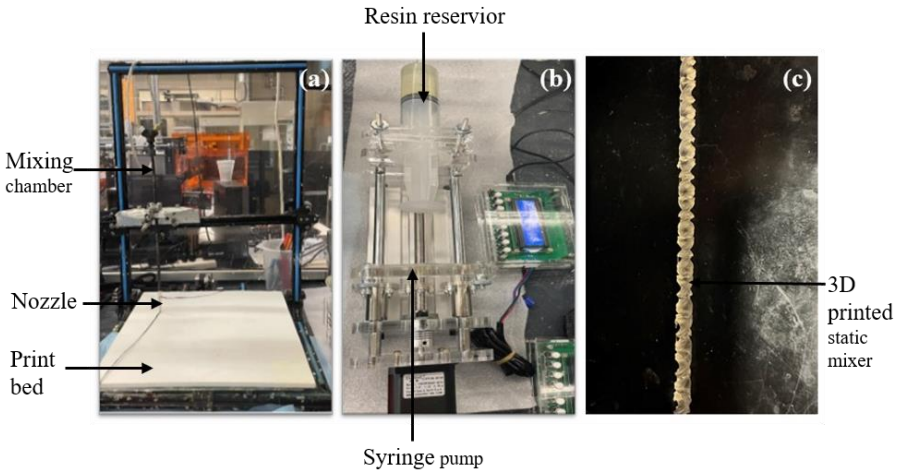

Figure 2: (a) ADIM lab gantry pro printer (b) Syringe pump (c) Static mixer.

The gantry of the AM printing system, as shown below in Figure 3 was modified in order to manufacture composites using a reactive resin system and continuous carbon fiber. The ShopBot gantry system was selected because of its bed size and open-source software. The gantry system was purchased from ShopBot Tools Inc. (Durham, North Carolina, USA) . It has dimensions of 1219.2 mm x 1219.2 mm. Cartridges, serving as reservoirs for resin and hardener, are positioned atop the gantry to allow the seamless flow of resin into the dispensing head system without disruptions. To regulate the resin flow, a pressure gauge is linked to the cartridges. The gantry is intricately designed to establish a connection between the resin-loaded cartridges and the Vipro head, which incorporates the pump mechanism.

This gantry system was designed to fabricate composites with large dimensions. It can move on all three axes (X, Y and Z). All three axes' motion were driven by a stepper motor. Aluminum print bed of 500 x 500 mm was used as a printing bed. To prevent any damage to the print bed during the removal of printed samples, masking tape was applied in the bed. G-code was manually written according to the geometry of test specimens. Subsequently, this manually written code was uploaded to the ShopBot control software version 3.8 (ShopBot Tools, Inc., Durham

NC). The software facilitated the successful printing of each specimen in accordance with its predefined parameters, including control over printing speed.

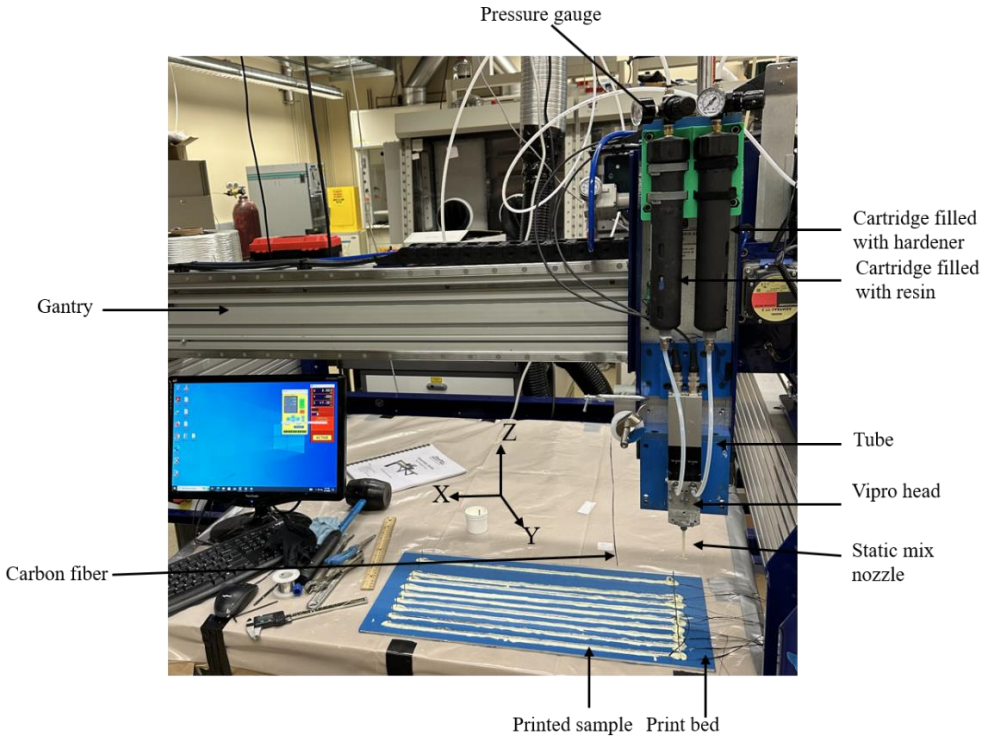

Figure 3: Printing system attached with ShopBot Gantry.

4.2.1. Resin Pumping System

A two-component print pump, Vipro-head (purchased from ViscoTec America Inc.), was used for dispensing the resins on the print bed. This print pump was installed on the head of ShopBot 3D printer gantry, and the drive units (stepper motor) of the pump were connected to the control unit to change flow rate of resins. This head consists of two dosing units for components A and B that work independently and can also be controlled individually. The print pump is a two-way progressive cavity pump, which consists of a rotating part known as a rotor, and a stator. Themaximum volume flow rate per dosing unit is 3.3 mL/min. The flow rate was controlled by the Arduino control unit or program. The mixing ratio range of this pump is 1:1 to 5:1, however, the previous syringe pump system had the capability of mixing ratio 2:1. The static mixer was

connected to the lower part of the printing head. This print head was easy to use and can be dismantled easily and quickly for cleaning purposes. This head was cleaned each time after the replacement of resins to prevent the unnecessary curing of the resins inside the head, which could also block the outlet port. This head was selected for this study because of its high range of mixing ratio, its high rate of repeat accuracy (>99%), high mixing performance and volumetric dosing feature, regardless of its viscosity.

4.2.2. Mixing of Two-Part Reactive Resin

A static mixing nozzle was used to mix the two-part resin and hardener together, triggering the polymerization reaction that completes after the material is deposited. A static mixing nozzle (Adhesive Dispensing Limited, United Kingdom) as shown in Figure 4 was used to mix the two-part reactive resin system. This mixer was selected as it's easy to use, luer lock connection which was easily fitted in the Vipro head and maintained laminar flow. It has 12 mixing elements, 74.0 mm length, an internal diameter of 3.2 mm and an outer diameter of 5.0 mm. The static mixer components, length, and diameter can be varied according to the application [21]. Moreover, the static mixer can be customized for applications with minimal pressure drop [16], [25].

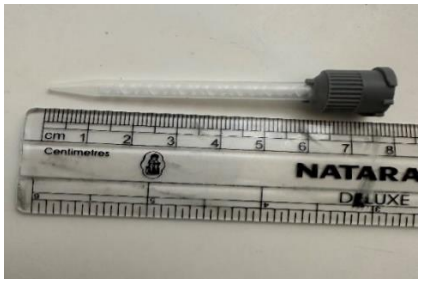

Figure 4: Static mixing nozzle.

4.2.3. Incorporation of Carbon Fiber with Reactive Resin

Referring Dallas Patton's thesis, a venturi nozzle was designed to dispense the mixed thermoset resins with the introduction of carbon fiber. Venturi nozzle was designed on the basis

of Bernoulli's principal, which states that within a steady flow of an incompressible, ideal fluid, the total energy per unit mass of the fluid remains constant along a streamline. Carbon fiber was introduced at the point where the low-pressure high velocity ends to minimize the resin backflow from the fiber inlet. The print properties and resolution depend on the nozzle geometry. Large diameter nozzles and exceedingly small diameter nozzles can result in an inappropriate fiber volume fraction ratio. Therefore, it depends on the size of individual fibers bundled together. The large diameter of nozzles and small tow size of carbon fiber can result in a low fiber volume fraction ratio. In contrast, the small diameter of nozzles and an exceptionally large tow size can result in a high fiber volume fraction ratio. The 3D model view of venturi nozzle used in this study is represented by Figure 5 (a)The outlet diameter of this nozzle was 3 mm. An inlet hole of 1 mm was made at the point of low pressure to feed the carbon fiber continuously into the resin system without the backflow of resins. The 3D designed venturi nozzle was printed using SLA printer. This venturi nozzle was attached with the static mixing chamber to introduce the carbon fiber with the help of Fevikwik gel as shown in Figure 5 (b).

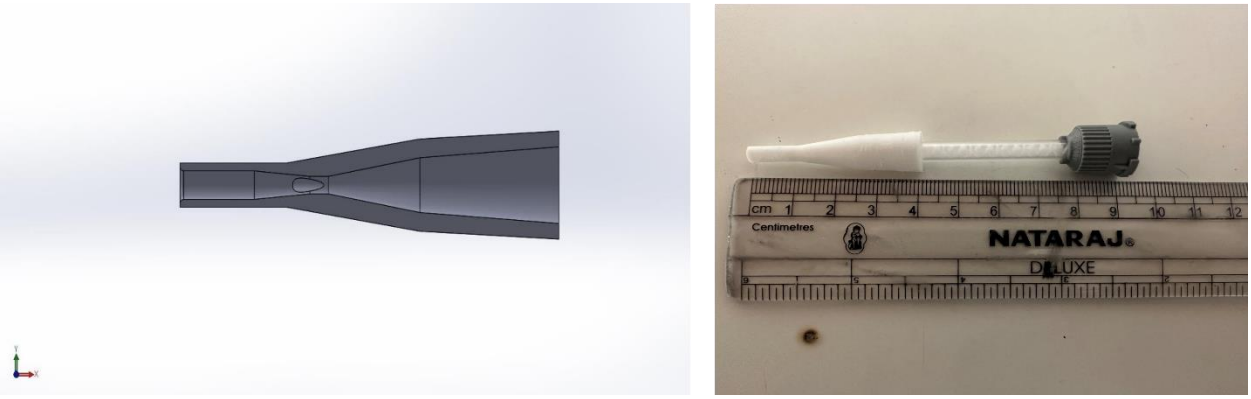

Figure 5: (a) 3D model of venturi nozzle, and (b) static mixing chamber attached with venturi nozzle.

5. PRINTING WITH CONTINUOUS FIBER

The samples were prepared according to the ASTM standard for tensile test and flexural test [42], [41]. Both neat and carbon fiber reinforced samples were printed for each resin system. The specimens printed were 400 mm long with 7 mm gap between the two lines. Specimens were then cut according to the dimensions required for each test. PX resin system samples were double layered. whereas Epon-Epikure resin system samples were of three layers. The specimen was printed with the lowest height possible to allow the bed to support each of the prints. Multiple trial prints were done by optimizing feed rate, flow rate and nozzle diameter to obtain a good composite sample. After multiple trials PX composites were printed successfully with the volumetric flow rate of 3.97 ml/min with the print speed of 1200 mm/min and Epon-Epikure composites were printed with the volumetric flow rate of 3.75 ml/min with the print speed of 1500 mm/min. The quality of the print was found to be dependent upon the mixing elements, flow rate feed rate, and nozzle design. Figure 6 depicts the printed sample of CCFR composite impregnated with (a) PX, and (b) Epon-Epikure resin system.

Figure 6: Composite samples printed with (a) PX, and (b) Epon-Epikure resin system.

Straight line print paths were used to print composites. It was observed that print failed during the turns where the fiber was pulled out of the bed. The resin was not able to hold the fiber during the convoluted sections, which made the resin flow over the bed. To overcome this problem, pins were attached to the print bed as shown in Figure 7 so that it could hold the fiber. Attaching pins on the bed and optimizing the G-code made the fiber hold during the print, which printed up to six layers.

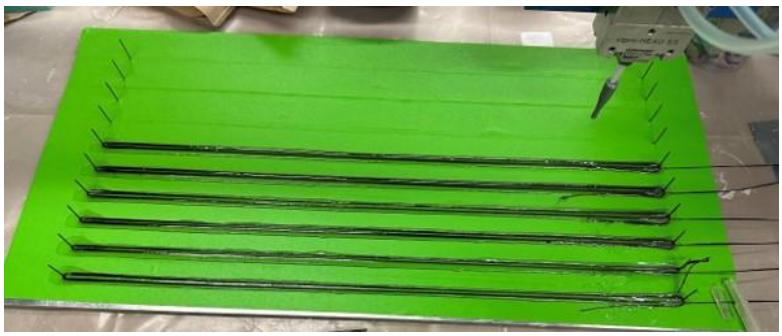

Figure 7: Pins attached to the print bed.

The cross-sectional images of the printed PX and Epon Epikure composite specimens were inspected using Keyence digital microscope (Keyence VHX-7000 (Itasca, IL)). The cross-section of the printed sample was polished to assess the better images. Figure 8 and 9 represents the microscopic cross-sectional view of printed PX and Epon Epikure composites respectively. In the figure, black circle dots are the carbon fiber. The big circle represents the void content in the sample. Figure 8 and 9 indicates the fiber being encompassed with the resin. This illustrates that a good wet out was obtained in both of the composite specimen.

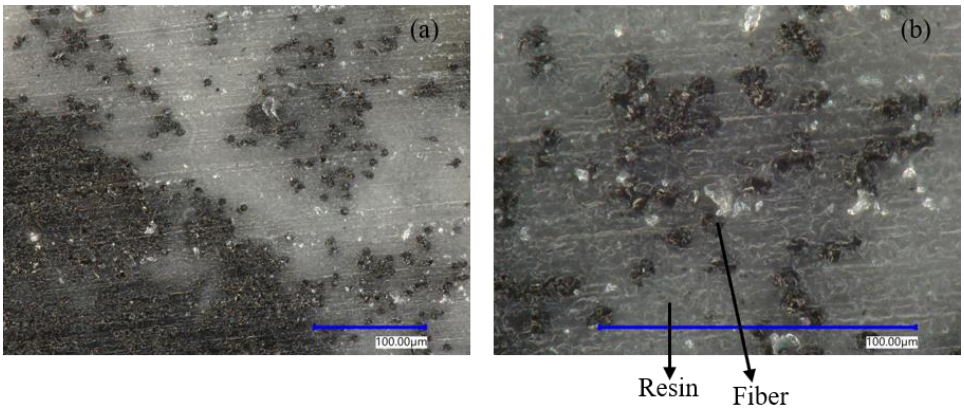

Figure 8: Cross-sectional image of PX composite with magnification level (a) X 2000 (b) X 700

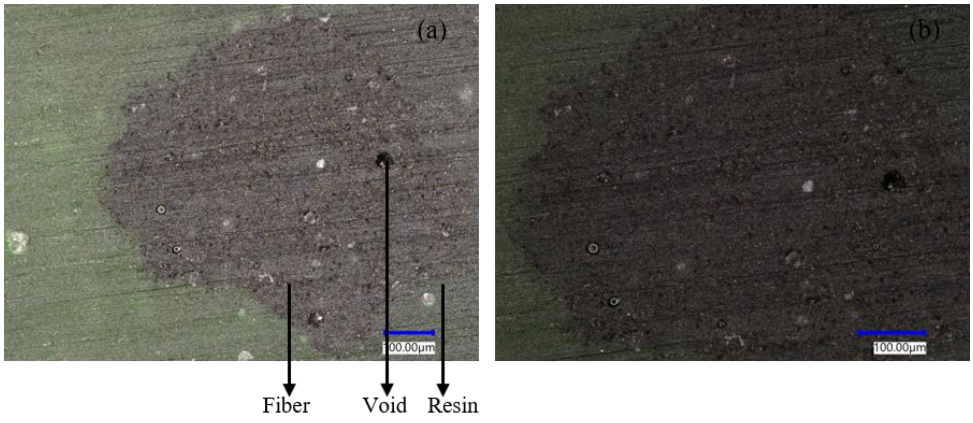

Figure 9: Cross-sectional image of Epon Epikure composite with magnification level (a) X 300 (b) X 400

Multiple custom resin systems developed by the NDSU Department of Coatings and Polymeric Materials were trialed before selecting the PX resin system. The selection process involved parameters such as gel time, material flow rate, curing of the resin system, bonding with carbon fiber, solidification of the sample and overall quality of the printed part. Initially, the resin system was printed without introducing the carbon fiber and its gel time, curing time, and print quality were observed. The flow rate was calculated as per the mixing ratio, and print speed was calculated using volumetric flow rate calculation and experimentation process. The experimental process concluded that the resin system was gelled inside the mixing chamber if the dispensing rate was too slow and did not cure properly when the dispensing rate was fast. The feed rate was also dependent on the flow rate. Both the parameters needed to be adjusted before the experimentation. After the resin system was able to dispense through the mixing nozzle successfully, carbon fiber was fed continuously to the system to develop composites. The excess flow of resins from the fiber inlet was observed instead of the nozzle outlet. The velocity of the resin system needed to be increased in the throttle section where carbon fiber was fed and decreased upon the nozzle's exit. Experimentation found that high-viscosity material provided a fine print of the composites rather than low-viscosity material. Less viscous material was found to flatten on the printing bed and back flow through the fiber inlet. The feed rate was optimized so that carbon fiber was strongly bonded with the matrix. The unusable resin system was found to have more gel time, which was not suitable to incorporate with carbon fiber. In total, five resin systems were evaluated, and the PX was selected, which performed well while incorporating carbon fiber with a mix ratio of 2.1 to 1, respectively. Table 4 depicts the list of resin systems trailed by their respective mixing ratio.

Table 4: List of Trial Resin System

Resin system	**Part 1 (Resin)**	**Part 2 (Hardener)**
Custom1	Pentaerythritol	M-Xylendiamine
Custom 2	Dipentaerythritol	M-Xylendiamine
Custom 3	Pentaerythritol	Furandiamine
Custom 4	TMP	M-Xylendiamine
Custom 5	Epon 8111	Epikure 3271

Figure 10 shows the flowchart diagram of the selection process of a usable resin system for custom resin. The commercial resin system Epon 8111 and Epikure 3271 resin system were selected due to its printability. Finally, after finding a desirable resin system that was able to print fine-resolution composites feeding the carbon fiber continuously, it was mechanically characterized, and it was compared with the neat resin system.

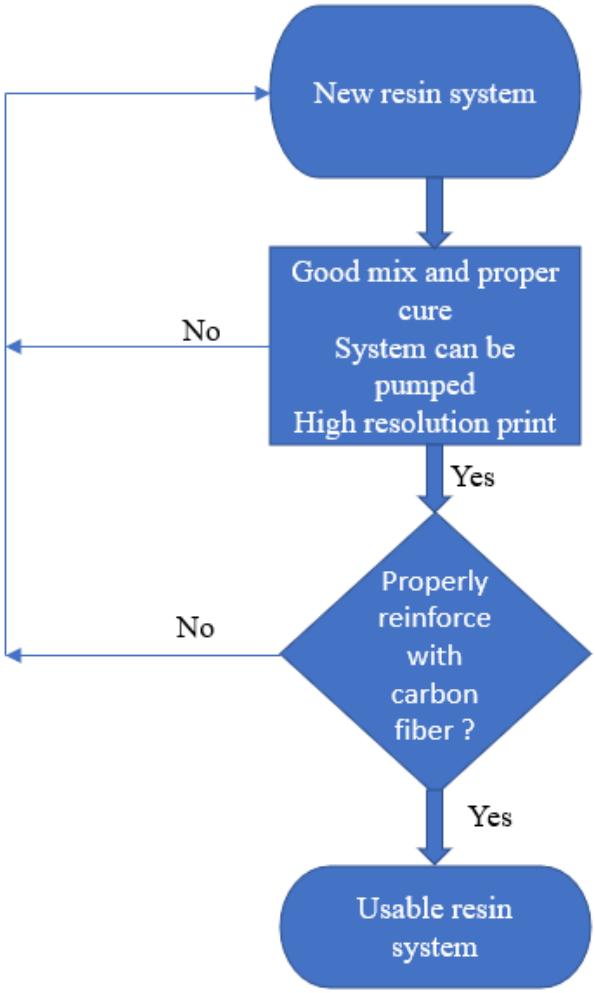

Figure 10: Approach for selecting usable resin system.

6. CHARACTERIZATION

6.1. Density Measurement

The densities of both the individual neat specimens and the composite materials were determined using ASTM D792 Method A [38]. Density calculations were performed using an Ohaus Adventurer TM scale AR2140 (Parsippany, New Jersey) and a Mettler Toledo Density Determination Kit 33360 (Greifensee, Zurich, Switzerland). Figure 11 illustrates the density test setup of composite. Distilled water was used in the beaker to perform the test. Initially, the mass of the specimen in air was measured using the weighing machine. Mass was recorded only after the specimen was left on the scale for 5 minutes. To ascertain the mass of the specimens while fully submerged, the dry specimen was carefully positioned onto the specimen holder before being immersed within the immersion vessel. Samples were then completely immersed in the liquid/distilled water, and their mass was measured after 5 minutes. The water temperature was measured with a thermometer, and its density was calculated. Equation 1 was used to calculate the density after the mass were weighted where D_1 is density, a is the dry mass of the polymer, b_1 is the apparent mass of the completely immersed specimen, and ρ_W is the density of water at 20.4 °C. The density of water was found to be 998.15 kg/m^3 at 20.4 °C

$$D_1 = \frac{\mathrm{a}}{\mathrm{a} - b_1} \times \rho_w \tag{1}$$

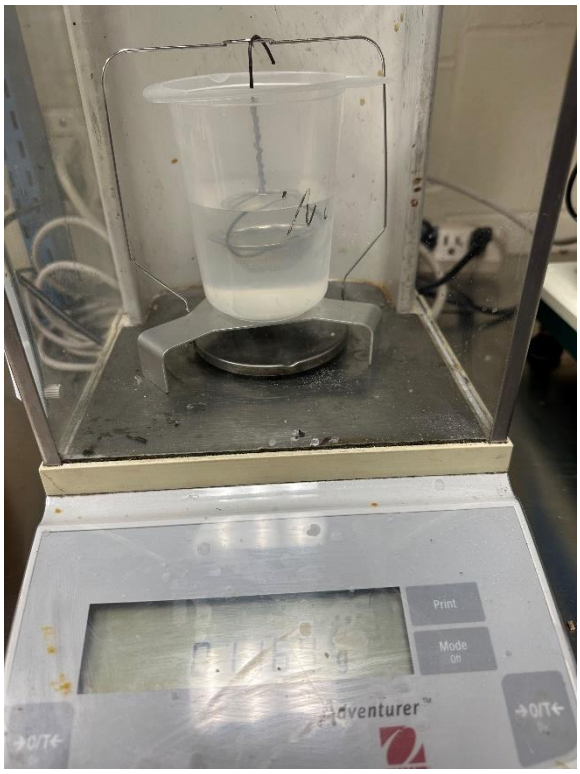

Figure 11: Density test setup for composite printed specimen.

6.2. Tensile Test

Tensile properties of the printed composites were determined by using the MTS Criterion Model 43 load frame as shown in Figure 12. Epon-Epikure samples were fully cured after 2 weeks of printing according to the supplier's data sheet. All the printed sample were tested after 2 weeks. The test was performed using ASTM standard ASTM D3039 [39] with 2.5 KN load cell. 25.4 mm extensometer was used on all neat and composite specimens to determine elongation and tensile modulus. The cross-head rate of the load frame used was 1 mm/min. 5 specimens of each resin type were tested. The specimen was printed as a rectangular bar with the dimensions as per the ASTM standard. For gripping of the tensile composite, they were tabbed on both sides. Tabs were attached using two-part epoxy glue.

Figure 12: MTS criterion model 43 load frame in tensile test setup.

Tensile strength, maximum load, and tensile elastic modulus were calculated using MTS criterion load frame. Stress was calculated by dividing the load with area. The area was measured for each sample with Keyence digital microscope (Keyence VHX-7000 (Itasca, IL)). Figure 13 represents the measurement of the cross-sectional area of irregular composites using Keyence microscope. The digital microscope provides more accurate and reliable measurements than any other caliper measurement. Image processing technology is accurately able to detect the edges of the object and calculate irregular areas which is critical to find by any other methods. Tensile elastic modulus was calculated after plotting the stress-strain data, which were taken from the

linear portion of the stress-strain curve. Equation 2 was used to calculate modulus where σ_t and ε_t are tensile stress and strain.

$$\mathrm{E} = \frac{\sigma_t}{\epsilon_t} \tag{2}$$

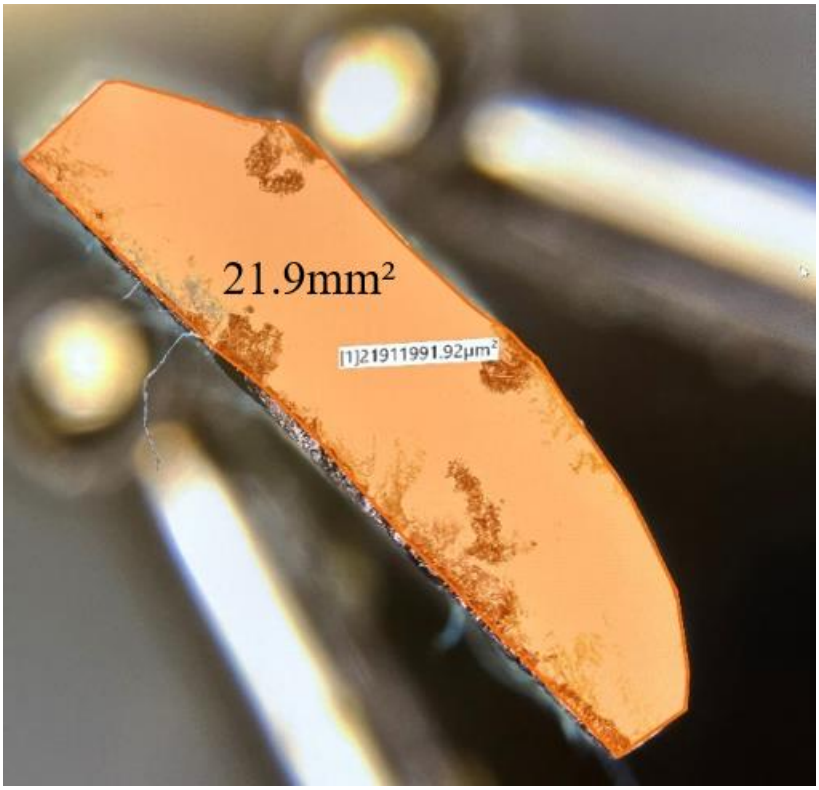

Figure 13: Area measurement of composite using digital microscope image.

6.3. Flexural Strength

Flexural testing was performed using a 3-point bending test to calculate the flexural strength and modulus according to ASTM D790 standard [40]. Flexural tests were performed using the same MTS Criterion load frame model number 43 with a 2.5kN load cell (Figure 14). The flexural specimen sample was printed according to the ASTM D790 standard, where the thickness was 3.20 mm, length was 75.75 mm and 12.70 mm wide. The span-to-thickness ratio of these samples was 16:1.

Equation 3 was used to calculate the flexural stress of the sample where *P* represents the load, *L* represents the span length, *b* represents the width of the beam, and *d* is the depth of the beam.

$$\sigma_f = \frac{3PL}{2bd^2} \tag{3}$$

Flexural strain and modulus were calculated by using the Equation 3 and 4 respectively, where *D* denotes the maximum deflection. $\sigma_{f1}$and σ_{f2} represent the flexural stress measurement taken at predefined points of the stress-strain curve, and $\epsilon_{f1}$and ϵ_{f2} are flexural strains measured at the same predefined points.

$$E_f = \frac{\sigma_{f1} - \sigma_{f2}}{\epsilon_{f1} - \epsilon_{f2}} \tag{4}$$

Figure 14: 3-point bend test setup.

6.4. Thermogravimetric Analysis

Thermal degradation temperature was determined by using the Thermogravimetric Analysis approach. This test was conducted according to the ASTM E1131 [41] standard using TGA 550 (TA instruments, New Castle, Delaware), as shown in Figure 15. Two samples of each resin system were cut, and the analysis was performed. Test were performed starting from 20 ºC to 600 ºC with a ramp rate of 10 ºC per minute. The char amount of composites were also calculated from the graph obtained from the TGA tests.

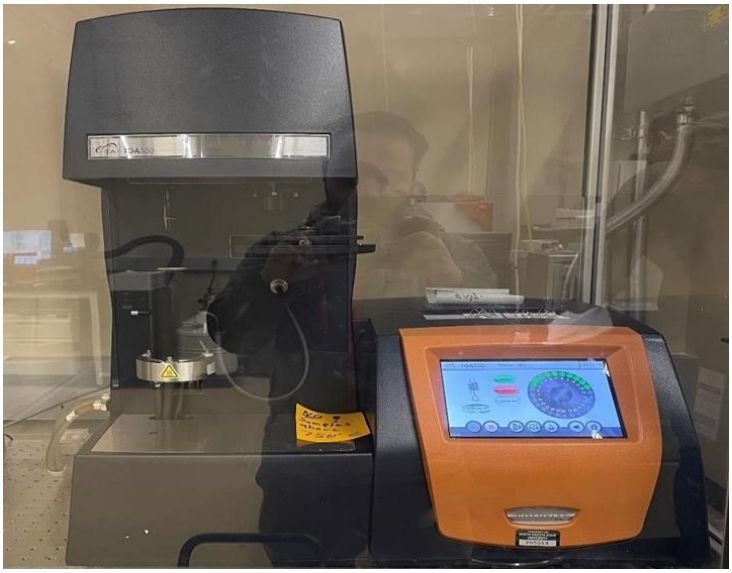

Figure 15: TGA 550.

6.5. Differential Scanning Calorimetry

To analyze the glass transition temperature of each printed specimen DSC test was performed. This test helps to prove the homogeneity of the mixture of resin system in the mixing chamber. DSC test was performed on the test apparatus DSC 2500 (TA instruments, New Castle, Delaware) as shown in Figure 16 and in reference to ASTM D3418 [41].

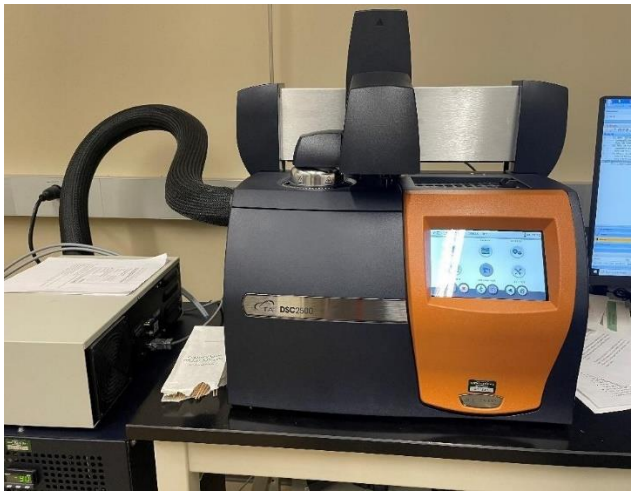

Figure 16: Differential scanning calorimetry apparatus 2500.

6.6. Burn-off Test

Burn-off test was conducted to find the fiber-volume ratio of the composites. Printed composites samples were cut into small sections and prepared for the Lucifer furnace to burn off the matrix materials. Figure 17 represents the Lucifer furnace apparatus. The composites were heated to 565 ˚C for 6 hours in the nitrogen environment. This test was conducted as per the standard ASTM D3171 [41]. Mass and density of each sample were measured before burn-off. Fiber-volume ratio was calculated based on the mass difference before and after burn-off. Equation 5 was used to calculate the fiber-volume fraction.

$$V_f = \frac{\frac{m_f}{\rho_f}}{\frac{m_f}{\rho_f} + \frac{m_m}{\rho_m}} \tag{5}$$

Where m_f and m_m represents mass of the fiber and matrix respectively and ρ_f and ρ_m denotes the densities of fiber and matrix respectively.

Figure 17: Lucifer furnace apparatus [42].

6.7. Micro CT

Micro CT scans was performed to find the void content on the printed composite samples. Micro CT tomographic images were used to find the volume of void content in the sample. Figure 18 represents the GE Micro CT Scanning system (Model: Phoenix vtomex s, Fairfield, CT, USA), at NDSU electron microscopy center which was used to perform the Micro CT scan.

Figure 18: GE MicroCT scanning system.

7. RESULTS AND DISCUSSION

7.1. Fiber-Volume Fraction

The fiber volume fraction of each composite was determined through theoretical and experimental methods. Initially, a theoretical approach was used to calculate the fiber-volume fraction. A small composite sample was prepared, and its dimensions and mass were recorded. Based on manufacturer's data sheet that the linear density of 3K tow continuous carbon fiber is 198 tex, which means 1000 m of 3K tow carbon fiber weights 198 gm. The overall mass of carbon fiber in the printed sample was calculated using linear density and its volume was determined by dividing the mass of the fiber with its density. The volume of the resin was also calculated by dividing the mass of the resin with its density. Equation 5 was employed to calculate the fiber volume fraction using this data, resulting in a fiber volume fraction of 2.15% for PX and 4.02% for the Epon-Epikure composite.

A burn-off test was then conducted to calculate the fiber volume fraction of continuous carbon fiber-reinforced PX Composite with two layers and Epon-Epikure composite consisting of 3 layers. In total, five small samples of each resin system were tested. This process effectively left the carbon fibers unburnt while carbonizing and/or creating volatiles of the resin matrix. During the burn-off test of these composites, the unburnt percentage of the matrix was also observed, and this percentage was calculated from the TGA test. The average mass of the samples tested was measured as 0.59 grams. The fiber volume fraction was subsequently calculated based on these masses and densities using Equation 5. The fiber volume fractions of the PX and Epon-Epikure composites were found to be 2.88 ± 0.16% and 4.42 ± 0.15%, respectively. Similarly, it is noteworthy that the fiber volume fractions calculated analytically and experimentally were found to be almost identical. However, a difference in fiber volume fraction was observed for printed

composites with PX and Epon-Epikure resin system. This difference was seen due to the different print parameters for each of the resin system. The flow rate and print speed used for printing two different composites were slightly different.

The theoretical minimum fiber volume fraction for each of the composite were calculated by using equation 3. If the fiber volume fraction is less than the minimum fiber volume fraction for any given composite, then the tensile strength of composite can be even lower than that of the matrix. The fiber present in the composite weakens the composite instead of strengthening and the matrix controls the composite failure when the fiber volume fraction is below the minimum fiber volume fraction.

$$V_{min} = \frac{\sigma_{mu} - (\sigma_m)_{\epsilon_{fu}}}{\sigma_{fu} + \sigma_{mu} - (\sigma_m)_{\epsilon_{fu}}} \quad (6)$$

Where σ_{mu} represents the ultimate matrix stress, $(\sigma_m)_{\epsilon_{fu}}$is the matrix stress at fiber fracture strain, σ_{fu} represents the ultimate fiber strength. The average minimum fiber volume fraction V_{min} of PX composite was found to be 0.15 % which is less than the experimentally gained fiber volume fraction of 2.88%. Similarly, the experimentally found fiber volume fraction of Epon-Epikure composite (4.42%) was also found higher than the minimum fiber volume fraction of 0.78%. This validates that the fibers carried load and the composite strength increased due to the continuous carbon fiber reinforcement.

7.2. Density Results

Density tests were performed on both the printed neat resin samples and the composite samples containing carbon fiber. For each resin system, the densities of 5 different specimens were calculated, and the resulting averages were determined. The specimens were initially weighed in

the air and then in distilled water, with their respective masses meticulously recorded. Densities were subsequently calculated based on the mass and volume of the samples, utilizing Equation 1.

Figure 19 (a) charts the densities of PX resin with and without carbon fiber reinforcement. The density of PX resin was 1.21 ± 0.03 g/cm^3, while density increased to 1.3 ± 0.01 g/cm^3 due to the incorporation of 2.88% carbon fiber volume fraction.

The densities of Epon-Epikure samples printed with and without carbon fiber reinforcement is depicted by Figure 19 (b). The density of printed Epon-Epikure sample without carbon reinforcement was 1.17 ± 0.015 g/cm^3 whereas the density of continuous carbon fiber reinforced Epon-Epikure sample with 4.42% fiber volume fraction was increased to 1.29 ± 0.011 g/cm^3.

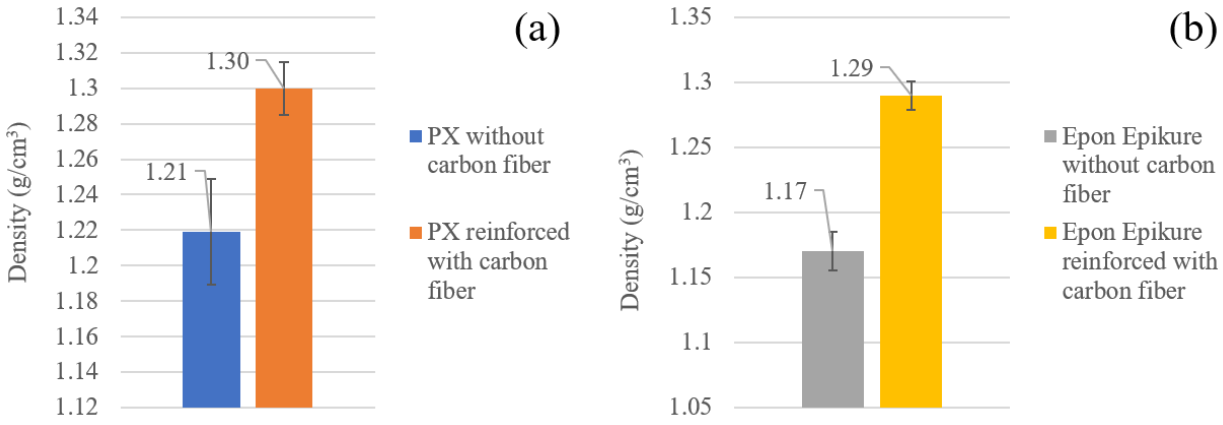

Figure 19. Densities of printed sample: (a) PX, and (b) Epon Epikure.

7.3. Tensile Properties

The objective of conducting tensile tests was to compare the change in tensile properties of the printed specimens with and without carbon fiber reinforcement. Figure 20 (a) and (b) represent the printed PX samples with and without carbon fiber reinforcement under tensile loading, respectively. Figure 21 (a) and (b) respectively depict the Epon-Epikure sample with and without carbon fiber reinforcement under tensile loading.

Figure 20: (a) PX printed composite sample, (b) PX neat sample under tensile loading.

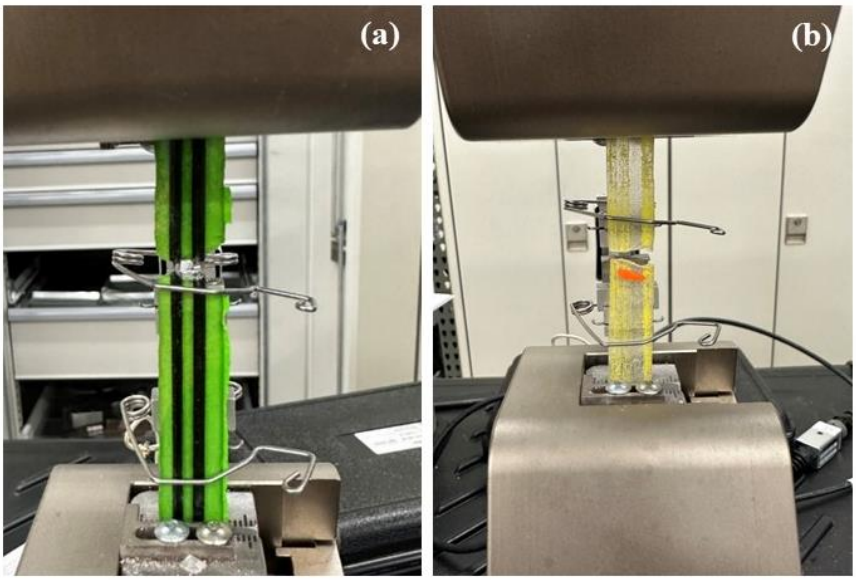

Figure 21: (a) Epon-Epikure composite under tensile loading, (b) Epon-Epikure neat sample.

Figure 22 (a) represents the average tensile strength of PX resin system with and without carbon fiber reinforcement. The tensile strength of PX resin sample with and without carbon fiber reinforcement was found to be 17.9 ± 1.90 MPa and 56.8 ± 4.22 MPa, respectively. Carbon fiber reinforced PX resin exhibited 217% increase in strength over neat PX resin sample.

Figure 22 (b) represents the average tensile strength of Epon-Epikure resin sample reinforced with and without carbon fiber. Epon-Epikure tensile strength was increased by 151% (52.08 ± 2.74 MPa to 130.74 ± 7.64 MPa) when reinforced with carbon fiber.

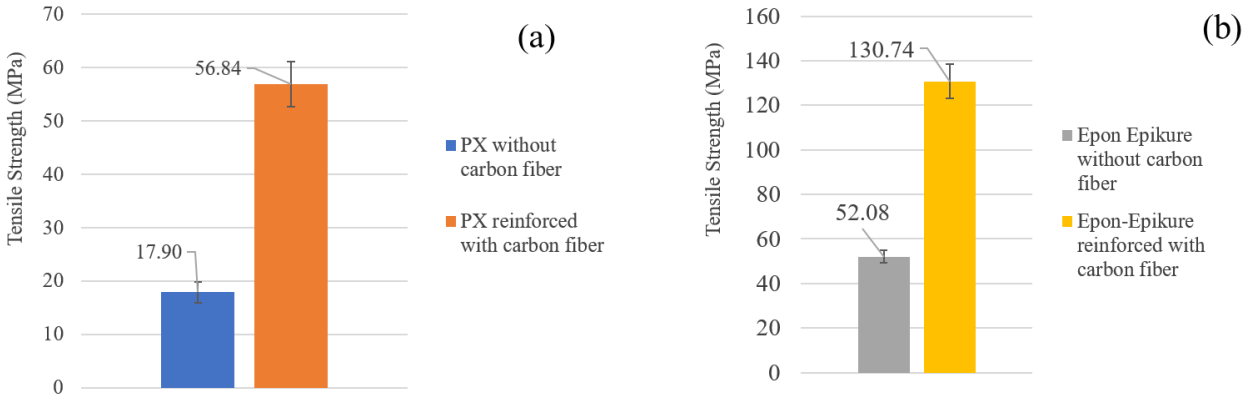

Figure 22: Tensile strength of printed samples: (a) PX and, (b) Epon-Epikure.

To determine the 3D printed composite stiffness, tensile modulus was calculated. Figure 23 (a) shows the tensile modulus of PX resin sample with and without the fiber reinforcement. The average tensile modulus of the printed PX resin was found to be 1.56 ± 0.40 GPa. An increase in the modulus of PX resin reinforced with continuous carbon fiber was observed. PX specimen reinforced with carbon fiber featured a 272.52% (1.56 ± 0.40 GPa to 5.83 ± 0.48 GPa) increment in tensile modulus over the PX neat resin.

Figure 23 (b) shows the tensile modulus of Epon-Epikure resin system with and without carbon fiber reinforcement. The average tensile modulus of printed Epon-Epikure resin was found to be 3.05 ± 0.23 GPa. Epon-Epikure resin reinforced with carbon fiber exhibited a 208.92% (3.05 ± 0.23 GPa to 9.45 ± 0.71 GPa) increment in tensile modulus.

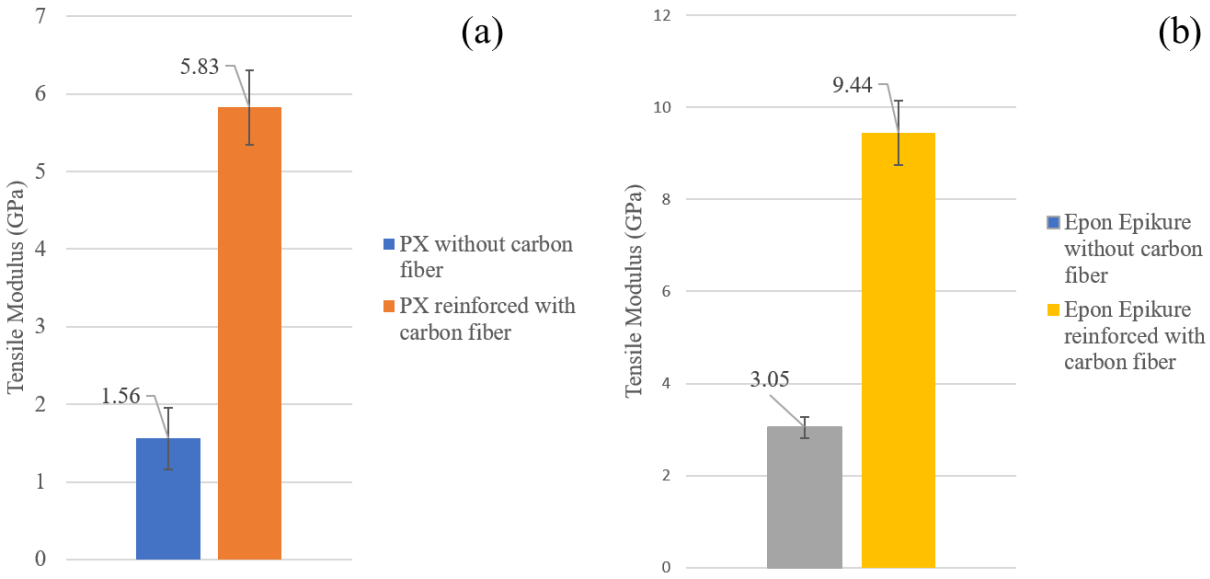

Figure 23: Average tensile modulus of (a) PX and, (b) Epon-Epikure resin sample.

A representative stress-strain curve of each resin system with and without continuous carbon fiber under tensile loading is depicted in Figure 24. Carbon fiber reinforced PX resin sample exhibited average failure strain of 0.01 ± 0.0011 mm/mm. It can be observed from the graph that the composite did not undergo any yielding or necking until the failure. The average strain-to-failure of the PX neat resin system was found at 0.02 ± 0.005 mm/mm. The average strain to failure of a matrix was found to be higher than the fiber. Similarly, the average strain to failure of 0.0228 ± 0.0014 mm/mm was found for Epon-Epikure matrix. Again, the strain to failure of neat resins was found higher than the strain to failure of carbon fiber reinforced composites.

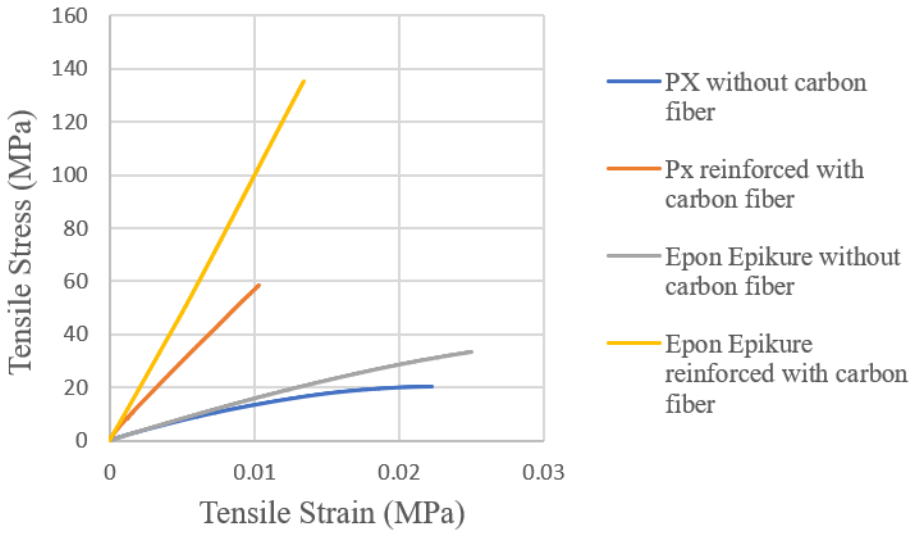

Figure 24: Representative stress vs strain graph under tensile loading.

Tensile strength and modulus of continuous carbon fiber reinforced composites were calculated theoretically using the rule of mixture as shown in equation 7 and 8.

$$\sigma_c = \sigma_f' V_f + \sigma_m (1 - V_f) \tag{7}$$

$$E_C = E_f V_f + E_m (1 - V_f) \tag{8}$$

Where σ_c and E_C represents the tensile strength and tensile modulus of the composites respectively, σ_m represents the tensile strength of matrix material. V_f represents the fiber-volume fraction of the composites. σ_f indicates the strength of carbon fiber at failure strain. According to the manufacturer's published data sheet, the strength and modulus of continuous carbon fiber for Toray,3k, are 3530 MPa and 230 GPa, respectively, with a failure strain of 1.5%. However, experimentally, the average strain to failure of printed carbon fiber reinforced samples was found to be 1%. This difference in strain was observed mainly due to the continuous rubbing of fiber in the tip of the nozzle. The strength value of carbon fiber at 1% strain was calculated as 2353 MPa by using the unitary method. As a result, the calculated strength and modulus values for the PX composite reinforced with carbon fiber are 68.11 MPa and 6.475 GPa, respectively.

Similarly, the strength and modulus of the carbon fiber reinforced Epon-Epikure samples was calculated as 144.59 MPa and 12.1 GPa, respectively. Nevertheless, the experimentally derived tensile strength and modulus values of PX composites exhibit a 16% and 9% lower values, respectively, in comparison to their corresponding theoretical values. Likewise, the strength and modulus values for Epon-Epikure samples with carbon fiber reinforcement showed a 9% and 21% lower values, respectively, in comparison to their respective theoretical values. This variation observed could be ascribed to the intrinsic constraints inherent in 3D-printed specimens, including voids and wet-out, testing conditions and misalignment of fibers in the composites.

From the tensile results it can be concluded that the % increase in strength and modulus of printed PX composite sample was higher than the Epon-Epikure sample despite having lower fiber-volume fraction of PX. Higher % increase in PX composite sample can be assumed due to the better compatibility and bonding between fibers and matrix. The fracture surface of specimen subjected to tensile test was captured using Scanning electron microscopy (SEM) to confirm this assumption.

The fracture surface of specimen subjected to tensile test was captured using Scanning electron microscopy (SEM). Figure 25 and 26 represents the SEM images of PX and Epon-Epikure sample with carbon fiber reinforcement. The impregnation of resin with carbon fiber can be observed from the figure. SEM image of both samples reveal that fiber pull-out was the primary mode of failure during the tensile loading. The images suggest that the PX resin has stronger bonding due to the presence of chips and jaggedness compared to smoother surfaces of Epon-Epikure. The stronger bonding indicated the better composite strength increase.

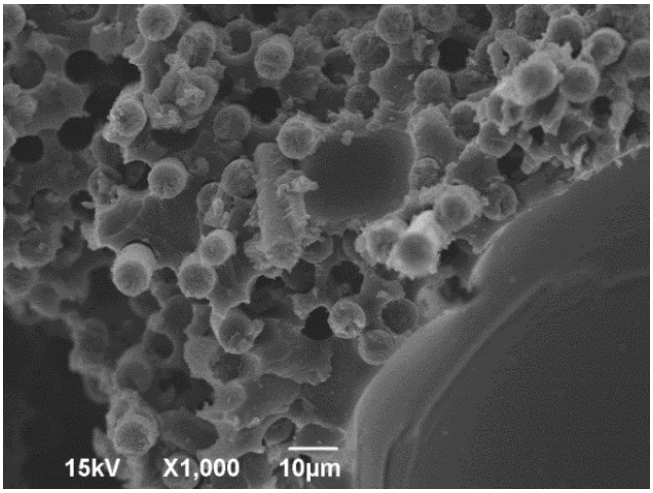

Figure 25: SEM images of PX specimen reinforced with carbon fiber.

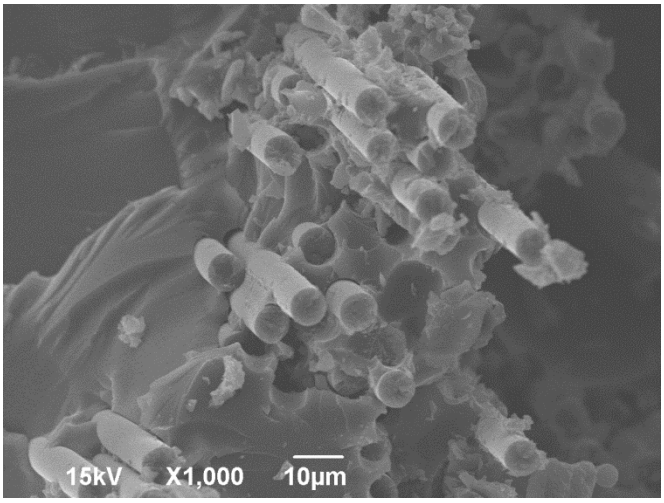

Figure 26: SEM images of Epon-Epikure specimen reinforced with carbon fiber.

7.4. Flexural Properties

The flexural properties of the printed samples were obtained by 3-point bending test. Figure 27 represents the representative PX specimen under flexural loading during 3-point bend test.

Figure 27: PX composite bending under flexural load.

Five specimens of each PX and Epon-Epikure resin system for neat and fiber reinforced composites were tested. Figure 28 represents the stress versus strain curve of PX resin system. It can be seen that matrix failed at 0.04 mm/mm and composite failed at 0.025 mm/mm with the maximum flexural stress at 97 MPa at maximum load of 100.57 N. Failure strain of matrix was found higher than the composite.

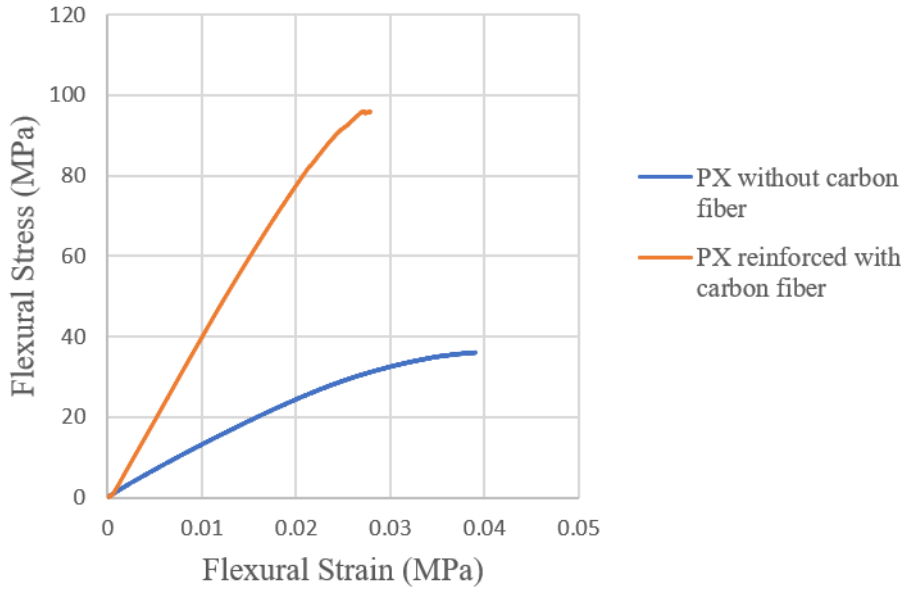

Figure 28: Flexural stress vs strain graph of PX resin system.

Similarly, the representative graph of flexural stress versus strain graph of Epon-Epikure printed sample with and without carbon fiber reinforcement is depicted by Figure 29. The printed samples without carbon fiber reinforcement exhibited flexural strain of 0.025 mm/mm. Carbon fiber reinforced samples showed strain of 0.023 mm/mm.

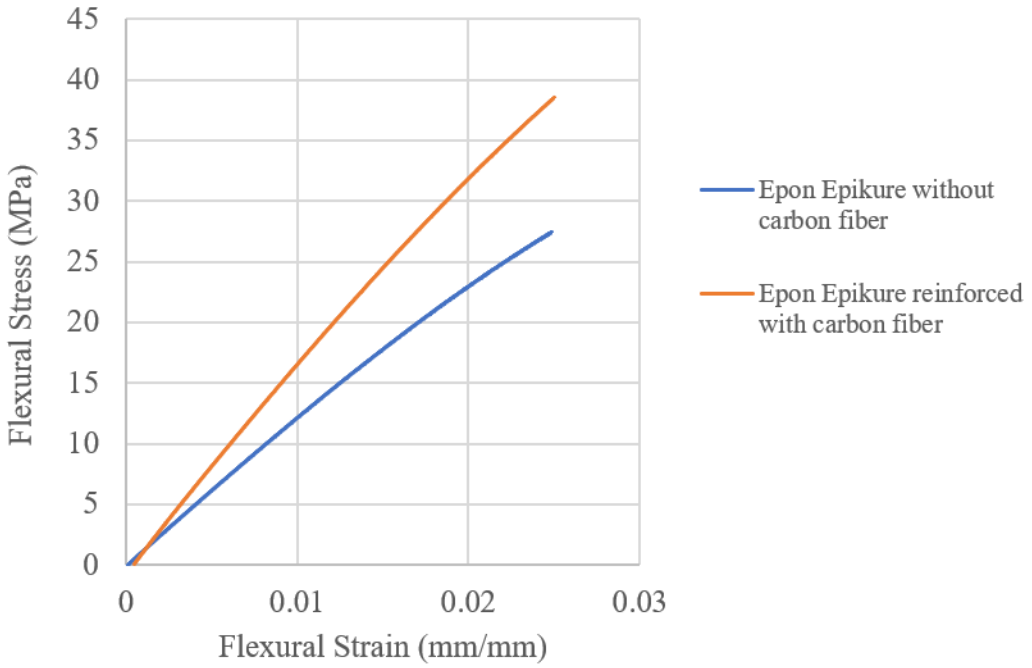

Figure 29: Flexural stress vs strain graph of Epon-Epikure resin system.

Figure 30(a) represents the average flexural strength of printed PX resin with and without carbon fiber reinforcement. The average flexural strength of PX resin with and without carbon fiber reinforcement was found to be 93.62 ± 8.90 MPa and 30.6 ± 6.58 MPa, respectively. It was found that PX composites increased flexural strength by 205% compared to printed PX neat resin, which was very similar to an increase in tensile strength. It can be analyzed that carbon-fiber reinforced PX sample showed a strong interfacial bonding with carbon fiber in longitudinal as well as transverse directions.

Figure 30 (b) represents the average flexural strength of printed Epon-Epikure resin with and without carbon fiber reinforcement. The average flexural strength of Epon-Epikure resin with and without carbon fiber reinforcement was found to be 33.80 ± 4.69 MPa and 44.84 ± 4.14 MPa, respectively. It can be seen that Epon Epikure composites increased flexural strength by 33.62% in comparison to printed sample with neat Epon Epikure resin system. Low increment of flexural

strength can be observed of Epon-Epikure resin reinforced with carbon fiber. The composite resistance to forces in various directions is strongly influenced by both the fiber orientation and quality of bonding.

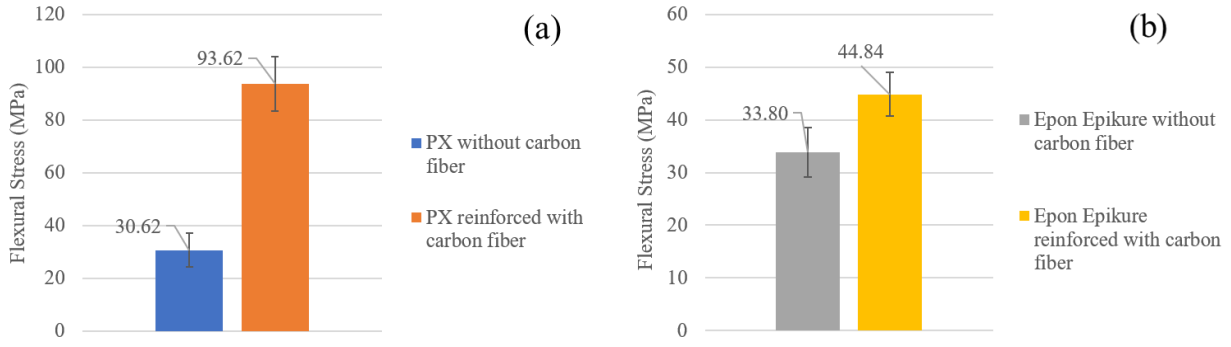

Figure 30: Average flexural stress of (a) PX and, (b) Epon-Epikure printed sample.

Figure 31 (a) represents the average flexural modulus of printed PX sample with and without carbon fiber reinforcement. The flexural modulus of printed PX sample without carbon fiber reinforcement was found to be 1.14 ±0.2 GPa. The increase of flexural modulus by 246% (1.14 ± 0.20 GPa to 3.95 ± 0.45 GPa) was observed when carbon fiber was introduced in PX resin sample.

Similarly, the flexural modulus of printed Epon-Epikure sample with and without carbon fiber reinforcement is depicted by Figure 31 (b). The modulus of Epon-Epikure sample was found to be 1.16 ± 0.20 GPa without carbon fiber reinforcement. The reinforcement of carbon fiber in the Epon-Epikure sample increased the modulus to 1.76 ± 50 GPa. 50% increase in flexural moudulus was observed with the carbon fiber reinforcement.

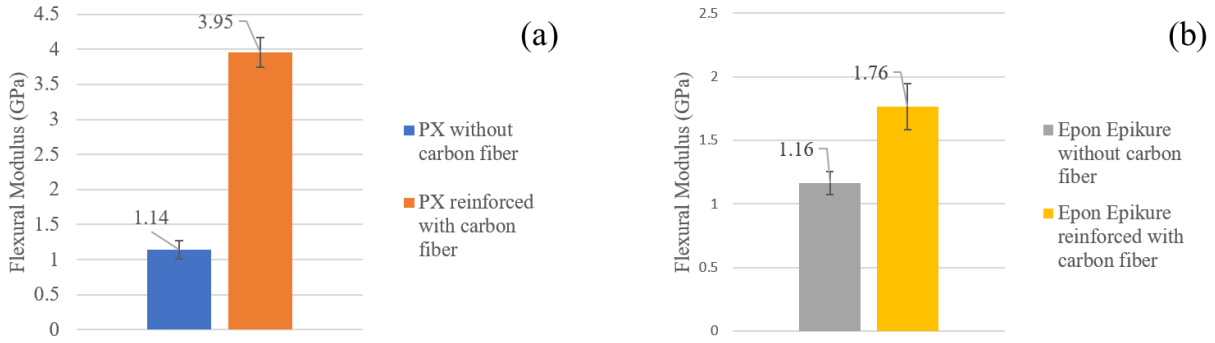

Figure 31: Average flexural modulus of (a) PX and, (b) Epon-Epikure printed sample.

The 3-point bend test results of PX and Epon-Epikure sample with and without carbon fiber reinforcement is tabulated below.

Table 5. 3-Point Bend Test Results of the Printed Samples.

3-Point bend	**Stress (MPa)**	**% Stress Difference**	**Flexural modulus (GPa)**	**% Modulus Difference**
PX neat	30.62 ±6.58	205.74	1.14± 0.20	246
Carbon fiber reinforced PX sample	93.62 ±8.90		3.95± 0.45	
Epon-Epikure neat	33.8 ±4.69	32.66	1.16±0.20	50
Carbon fiber reinforced Epon-Epikure sample	44.84 ±4.14		1.76±0.55	

The flexural fracture surfaces of the printed composites were analyzed with microscopic imaging using Keyence digital microscope ((Keyence VHX-7000 (Itasca, IL)). Fracture surfaces of PX and Epon Epikure composites are shown in Figure 32 and 33 respectively. Different fiber pull out lengths can be observed from the images. The fibers are more centralized on the Epon Epikure composites. In PX composite fibers are layed on the surfaces.

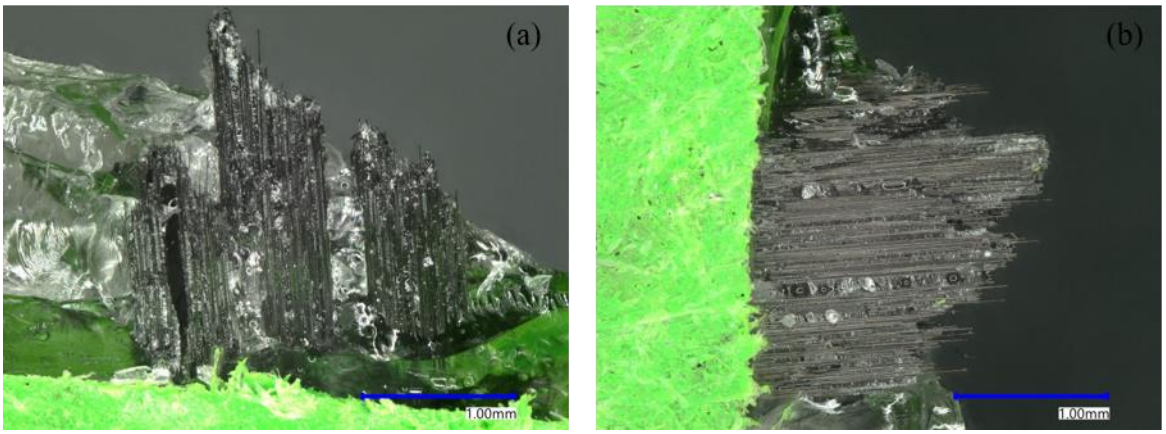

Figure 32: Microscopic image of flexural fracture Epon Epikure composite sample (a) cross-section (b) bottom surfaces.

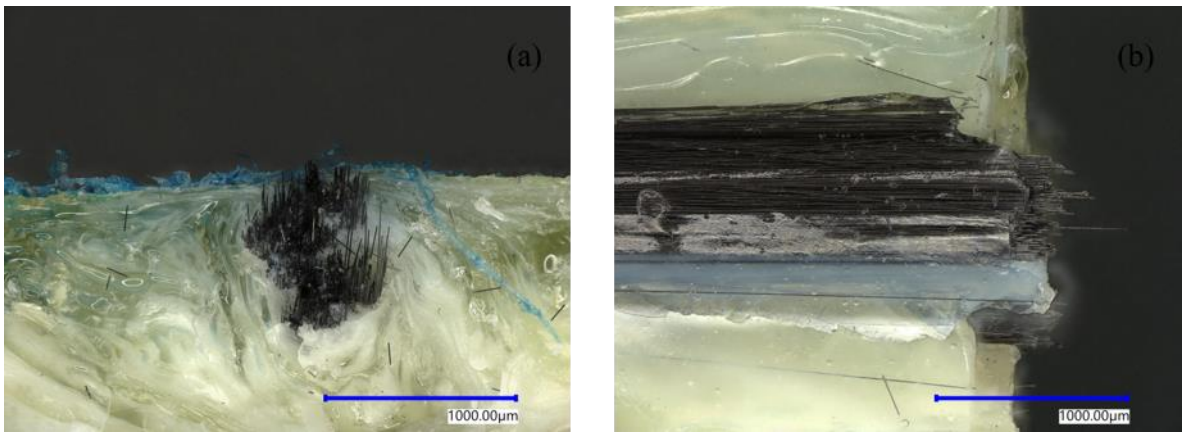

Figure 33: Microscopic images of flexural fracture PX composite sample (a) cross-section (b) bottom surfaces.

7.5. Viscosity Measurement

The viscosity of each resin and amine were analyzed by using an ARES G2 rotational rheometer (TA Instruments, DE, USA). This test was performed placing the resin or amine between two stainless steel fixtures with parallel plates, each having a diameter of 25 mm, and maintaining a gap of 0.5 mm between them. The test was performed at ambient room temperature of 25 ºC. The viscosity of mixed resin and amine was measured using viscosity dip cup (Elcometer Inc, Warren, MI) at room temperature. The viscosity of each resin and amine are tabulated below.

Table 6: Viscosity of Resin and Amine.

Sample	Viscosity (Centipoise)
Pentaerythritol	616.75
M-Xylendiamine	8.06
Epon 8111	820
Epikure 3271	110
Mixed PX resin system	500
Mixed Epon Epikure resin system	957.21

7.6. Thermogravimetric Analysis

The TGA test was performed to find the thermal stability of the PX and Epon-Epikure resin system. The onset temperature of thermal degradation of printed neat PX and Epon-Epikure sample was found to be 276 ℃ and 330 ℃, respectively. Furthermore, TGA was performed with carbon fiber reinforcement to establish the effect of carbon fiber on degradation temperature. With the carbon fiber reinforcement, the onset temperature decreased from 276 ℃ to 270 ℃ for PX sample. Similarly, the onset temperature was 332 ℃ for Epon-Epikure sample, with the carbon fiber reinforcement. Figure 34 depicts the representative TGA curve of PX sample reinforced with continuous carbon fiber. Both PX and Epon-Epikure resin system exhibit relatively high thermal degradation temperature.

The residual weight was the weight of carbon fiber as well as some portion of matrix which was not fully burned (i.e. char). This was found out while performing burn-off test. The residual weight % of PX composite was approximately 23%.

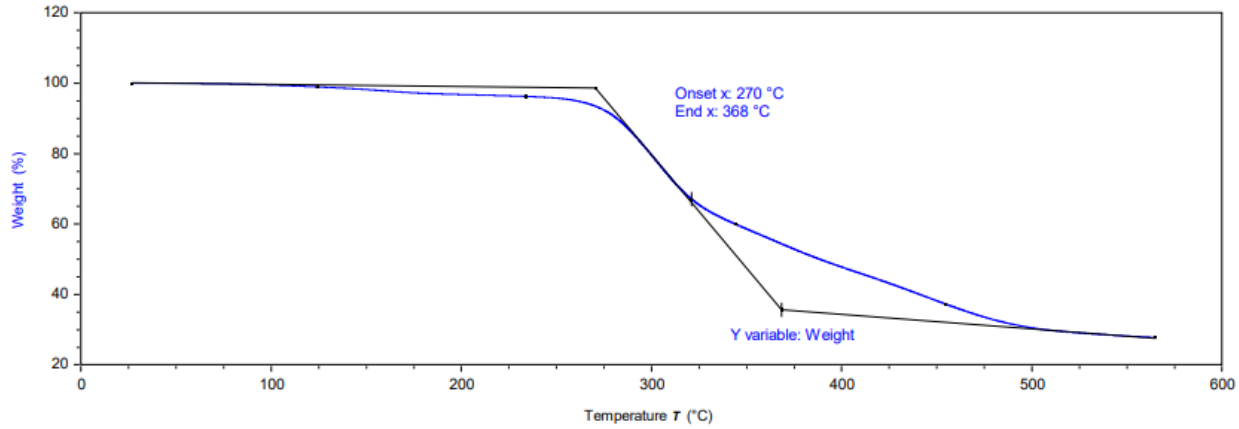

Figure 34: TGA curve of PX printed composite.

Similarly, the representative TGA curve of printed Epon-Epikure sample reinforced with carbon fiber is represented by Figure 35. The average residual weight % of the Epon-Epikure printed composite was found to be 20%.

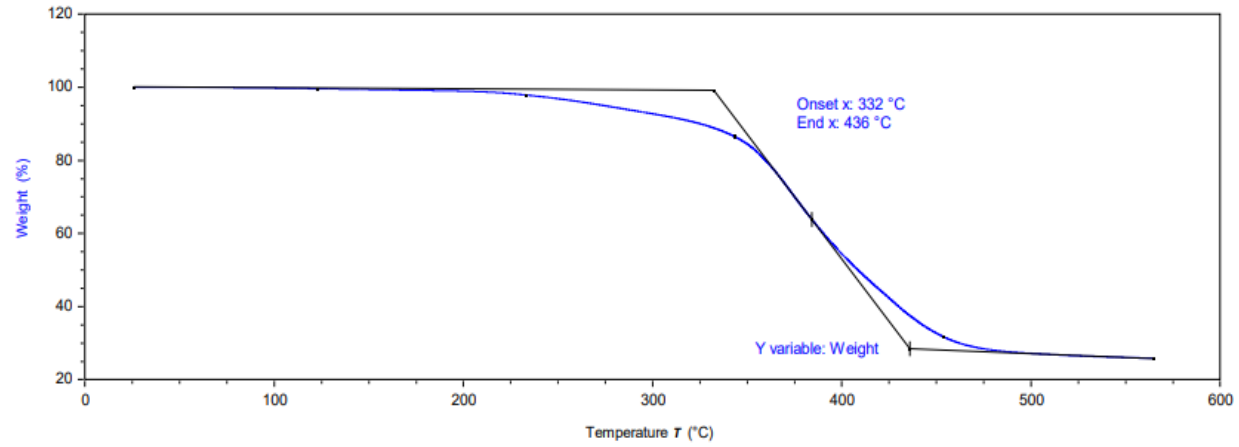

Figure 35: TGA curve of Epon-Epikure reinforced carbon fiber sample.

7.7. Differential Scanning Calorimetry

The objective of performing DSC test was to find the glass transition temperature of two different resin systems. DSC was performed on both 3D printed sample using PX and Epon Epikure resin system. The glass transition temperature for PX sample with and without carbon fiber was found to be 59 °C and 58 °C respectively. Similarly, glass transition temperature for

Epon Epikure sample with and without carbon fiber was found to be 48.3 °C and 52 °C respectively. Carbon fiber reinforced samples did not show any significant difference in glass transition temperature in comparison to printed samples without fiber reinforcement. This negligible difference could be due to the low fiber volume fraction. Glass transition temperature was increased during the second heating during DSC test. It can be assumed that the samples were not fully cured and required post curing for both PX and Epon Epikure samples.

7.8. Micro CT Testing

The mechanical properties are varied by the void content in the printed composite samples. Micro CT scan was performed for both PX and Epon Epikure composites to determine the void content. To measure the void content inside the PX composite, 245 mm^3 by volume printed sample with 12.6 mm long and 7.29 mm width sample was tested. Figure 36 represents the sample void distribution from the Micro CT images. The void content in the tested PX sample was found to be 1.40%.

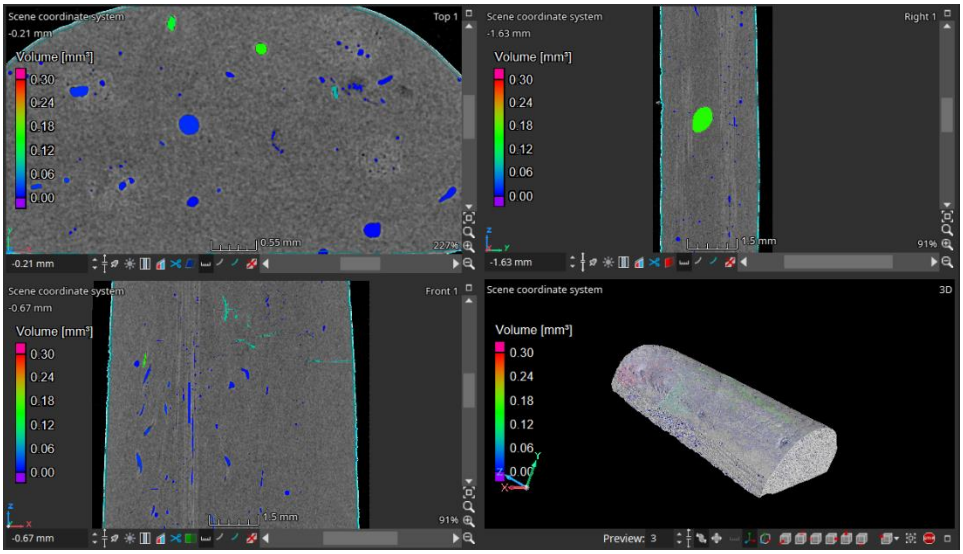

Figure 36: Micro CT of printed PX composite sample.

Similarly, tested Epon Epikure sample was 12 mm long, 8.66 mm wide with the volume of 156 mm^3. Figure 37 represents the void distribution in Epon Epikure composites from the Micro CT images. The overall void content in the sample was found to be 2.90% with the volume of 4.65 mm^3.

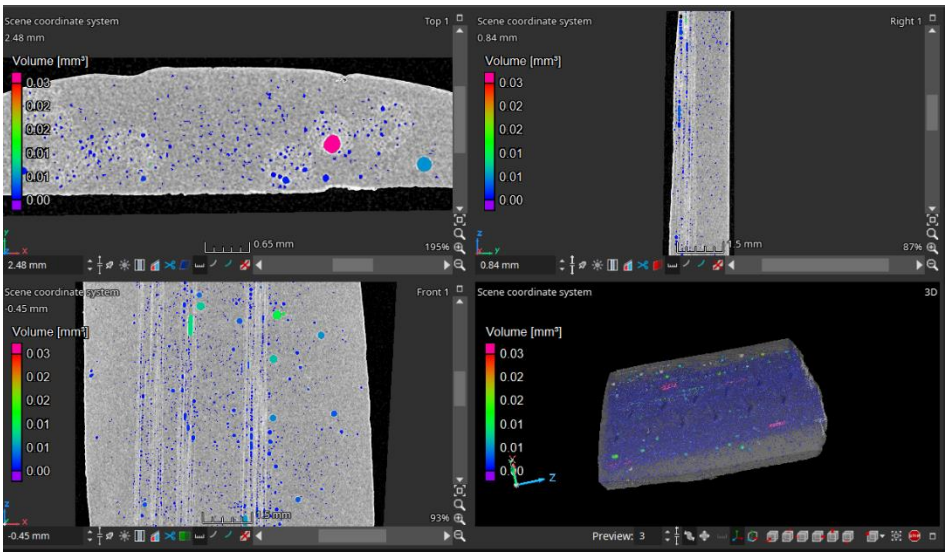

Figure 37: Micro CT of printed Epon-Epikure composite sample.

8. CONCLUSION

A 3D printing system was developed successfully to manufacture continuous carbon fiber reinforced composites utilizing two-part reactive resins. Effective mixing between resin and hardener was achieved by using a dual progressive cavity pump and static mixing nozzle. Carbon fiber was successfully introduced into the resin system using venturi nozzle. Samples were printed successfully using the PX resin system and the commercial Epon Epikure epoxy resin system. The fiber-volume fraction was analyzed using burn-off test and analytical approach. Fiber volume fraction of printed carbon fiber reinforced PX and Epon Epikure resin system were obtained as 2.88% and 4.42% respectively through burn-off test. Similarly, fiber-volume fraction was calculated as 2.15% and 4.05%by analytical approach.

The mechanical properties of each printed sample were increased with the continuous carbon fiber reinforcement. The tensile strength and modulus of printed PX sample increased by 217% and 272.5%, respectively when reinforced with 2.8% carbon fiber volume content. Similarly, Epon Epikure sample also showed increment in tensile strength and modulus by 151% and 208%, respectively with 4.2% carbon fiber volume. In addition to this, carbon fiber reinforced samples exhibited increment in flexural properties for both PX and Epon Epikure resin system. Flexural strength of PX and Epon Epikure sample increased by 205% and 32.6%, respectively, compared to neat PX and Epon Epikure sample. Moreover, flexural modulus of PX and Epon Epikure sample was increased by 246% and 50% with the continuous carbon fiber reinforcement. Neat 3D printed samples showed a thermal degradation temperature of 275 °C and 330°C for PX and Epon Epikure resin system, respectively. The thermal degradation temperature of printed PX and Epon Epikure samples with carbon fiber reinforcement was found to be 270 °C and 332 °C, respectively. Slight decrease in degradation temperature was observed compared with neat resin

sample. Since carbon fiber itself has the higher mechanical properties, the resin system used in this research exhibited significant increment in mechanical properties when reinforced with continuous carbon fiber. The successful incorporation of continuous carbon fiber reinforcement through REAM process using reactive resins demonstrates a versatile manufacturing technique. This flexibility allows the creation of complex geometries and customized components, expanding the range of potential engineering applications. The substantial increase in tensile strength and modulus, as well as flexural strength and modulus, in the carbon fiber reinforced printed samples indicates that these materials have potential to offer significantly enhanced mechanical properties.

9. FUTURE RECOMMENDATIONS

The findings derived from this study offer opportunities for extension and optimization. The geometry of the nozzle could be further optimized to decrease the frying of carbon fiber in the nozzle, which decreases the mechanical properties of the composite. This study included PX and Epon-8111, Epikure-3271 resin system. Further study can also be done by adding the catalyst or thickening agent in the resin system to increase its viscosity. This printing system offers the potential for the exploration of novel resin systems in future research. Remarkable improvements in mechanical properties are evident, even at relatively low fiber-volume content. Future investigations may involve augmenting the fiber-volume fraction, minimizing inter-fiber gaps, and upgrading the carbon fiber tow from 3k to 6k, thereby enhancing the fiber volume fraction and, subsequently, the mechanical properties of the composites. This study involved the use of Toray 3k tow carbon fiber; however, future research may explore the comparative analysis of mechanical properties by employing different types of fiber. In the current study, specimens were printed under room temperature conditions. Further study could be conducted by printing the composite samples in a pre-heated printing bed. Further study can also be conducted by optimizing the printing process parameters like printing speed, layer thickness, and flow rate.

10. REFERENCES

[1] A. A. Alogla, M. Baumers, C. Tuck, and W. Elmadih, “The impact of additive manufacturing on the flexibility of a manufacturing supply chain,” *Appl. Sci.*, vol. 11, no. 8, 2021, doi: 10.3390/app11083707.

[2] Grand View Research, “3D Printing Market Size, Share & Trends Analysis Report By Component (Hardware, Software, Services), By Printer Type, By Technology, By Software, By Application, By Vertical, By Region, And Segment Forecasts, 2023 - 2030,” 202AD. [Online]. Available: https://www.grandviewresearch.com/industry-analysis/3d-printing-industry-analysis

[3] G. D. Goh *et al.*, “Characterization of mechanical properties and fracture mode of additively manufactured carbon fiber and glass fiber reinforced thermoplastics,” *Mater. Des.*, vol. 137, pp. 79–89, 2018, doi: 10.1016/j.matdes.2017.10.021.

[4] X. Wang, M. Jiang, Z. Zhou, J. Gou, and D. Hui, “3D printing of polymer matrix composites: A review and prospective,” *Compos. Part B Eng.*, vol. 110, pp. 442–458, 2017, doi: 10.1016/j.compositesb.2016.11.034.

[5] P. Parandoush and D. Lin, “A review on additive manufacturing of polymer-fiber composites,” *Compos. Struct.*, vol. 182, pp. 36–53, Dec. 2017, doi: 10.1016/J.COMPSTRUCT.2017.08.088.

[6] T. J. Horn and O. L. A. Harrysson, “Overview of current additive manufacturing technologies and selected applications,” *Sci. Prog.*, vol. 95, no. 3, pp. 255–282, 2012, doi: 10.3184/003685012X13420984463047.

[7] H. Prajapati, S. S. Salvi, D. Ravoori, M. Qasaimeh, A. Adnan, and A. Jain, “Improved print quality in fused filament fabrication through localized dispensing of hot air around the deposited filament,” *Addit. Manuf.*, vol. 40, p. 101917, Apr. 2021, doi: 10.1016/J.ADDMA.2021.101917.

[8] J. P. Kruth, G. Levy, F. Klocke, and T. H. C. Childs, “Consolidation phenomena in laser and powder-bed based layered manufacturing,” *CIRP Ann.*, vol. 56, no. 2, pp. 730–759, Jan. 2007, doi: 10.1016/J.CIRP.2007.10.004.

[9] C. W. Hull, "Apparatus for Production of Three-Dimensional Objects by Stereolithography," United States Patent, Appl., No. 638905, filed in 1984.

[10] O. A. Mohamed, S. H. Masood, and J. L. Bhowmik, “Optimization of fused deposition modeling process parameters: a review of current research and future prospects,” *Adv. Manuf.*, vol. 3, no. 1, pp. 42–53, 2015, doi: 10.1007/s40436-014-0097-7.

[11] P. K. Penumakala, J. Santo, and A. Thomas, “A critical review on the fused deposition modeling of thermoplastic polymer composites,” *Compos. Part B Eng.*, vol. 201, p. 108336, Nov. 2020, doi: 10.1016/J.COMPOSITESB.2020.108336.

[12] L. E. Fithian, “Where thermoplastic elastomers do and don’t fit vs. conventional rubbers,” *J. Elastomers Plast.*, vol. 14, no. 4, pp. 222–235, 1982, doi: 10.1177/009524438201400403.

[13] T. A. Lima *et al.*, “High-performance thermosets for additive manufacturing,” *Innov. Emerg. Technol.*, vol. 10, 2023, doi: 10.1142/s2737599423300039.

[14] M. A. Rahman, E. Hall, L. Gibbon, M. Z. Islam, C. A. Ulven, and J. J. La Scala, “A Mechanical Performance Study of Dual Cured Thermoset Resin Systems 3D-Printed with Continuous Carbon Fiber Reinforcement,” *Polymers (Basel).*, vol. 15, no. 6, 2023, doi: 10.3390/polym15061384.

[15] G. Zak, M. N. Sela, V. Yevko, C. B. Park, and B. Benhabib, “Layered-Manufacturing of Fiber- Reinforced Composites,” vol. 121, no. July 1998, 2019.

[16] O. Uitz, P. Koirala, M. Tehrani, and C. C. Seepersad, “Fast, low-energy additive manufacturing of isotropic parts via reactive extrusion,” *Addit. Manuf.*, vol. 41, p. 101919, May 2021, doi: 10.1016/J.ADDMA.2021.101919.

[17] J. K. Fink, “Reactive Polymers: Fundamentals and Applications,” *React. Polym. Fundam. Appl. A Concise Guid. to Ind. Polym.*, pp. 1–687, 2017, doi: 10.1016/C2017-0-01641-5.

[18] F. L. Jin, X. Li, and S. J. Park, “Synthesis and application of epoxy resins: A review,” *J. Ind. Eng. Chem.*, vol. 29, pp. 1–11, Sep. 2015, doi: 10.1016/J.JIEC.2015.03.026.

[19] J. O. Akindoyo, M. D. H. Beg, S. Ghazali, M. R. Islam, N. Jeyaratnam, and A. R. Yuvaraj, “Polyurethane types, synthesis and applications-a review,” *RSC Adv.*, vol. 6, no. 115, pp. 114453–114482, 2016, doi: 10.1039/c6ra14525f.

[20] O. Rios, W. Carter, C. Kutchko, D. Fenn, and K. Olson, “Evaluation of advanced polymers for additive manufacturing,” *ORNL Rep.*, vol. ORNL/TM-20, 2017.

[21] R. K. Thakur, C. Vial, K. D. P. Nigam, E. B. Nauman, and G. Djelveh, “Static Mixers in the Process Industries—A Review,” *Chem. Eng. Res. Des.*, vol. 81, no. 7, pp. 787–826, Aug. 2003, doi: 10.1205/026387603322302968.

[22] Chris. Rauwendaal, “Mixing in Polymer Processing (rauwendaal).pdf.” p. 475, 1991.

[23] A. C. Y. Wong and Y. Lam, “Visualization study on the dynamic mixing quality during single-screw extrusion,” *J. Polym. Res.*, vol. 15, no. 1, pp. 11–19, 2008, doi: 10.1007/s10965-007-9138-2.

[24] O. Uitz *et al.*, “Reactive extrusion additive manufacturing (REAM) of functionally graded, magneto-active thermoset composites,” *Addit. Manuf.*, vol. 67, p. 103486, Apr. 2023, doi: 10.1016/J.ADDMA.2023.103486.

[25] S. K. Romberg, C. J. Hershey, J. M. Lindahl, W. Carter, B. G. Compton, and V. Kunc, “Large-scale additive manufacturing of highly exothermic reactive polymer systems,” *Int. SAMPE Tech. Conf.*, vol. 2019-May, 2019, doi: 10.33599/nasampe/s.19.1616.

[26] L. W. Zhang, A. O. Sojobi, and K. M. Liew, “Sustainable CFRP-reinforced recycled concrete for cleaner eco-friendly construction,” *J. Clean. Prod.*, vol. 233, pp. 56–75, 2019, doi: 10.1016/j.jclepro.2019.06.025.

[27] X. Sun, F. Meng, J. Liu, J. McKechnie, and J. Yang, “Life cycle energy use and greenhouse gas emission of lightweight vehicle – A body-in-white design,” *J. Clean. Prod.*, vol. 220, pp. 1–8, 2019, doi: 10.1016/j.jclepro.2019.01.225.

[28] M. Ateeq, M. Shafique, A. Azam, and M. Rafiq, “A review of 3D printing of the recycled carbon fiber reinforced polymer composites: Processing, potential, and perspectives,” *J. Mater. Res. Technol.*, vol. 26, pp. 2291–2309, 2023, doi: 10.1016/j.jmrt.2023.07.171.

[29] R. Matsuzaki *et al.*, “Three-dimensional printing of continuous-fiber composites by in-nozzle impregnation,” *Sci. Rep.*, vol. 6, no. February, pp. 1–7, 2016, doi: 10.1038/srep23058.

[30] A. Imeri, I. Fidan, M. Allen, D. A. Wilson, and S. Canfield, “Fatigue analysis of the fiber reinforced additively manufactured objects,” *Int. J. Adv. Manuf. Technol.*, vol. 98, no. 9–12, pp. 2717–2724, 2018, doi: 10.1007/s00170-018-2398-7.

[31] J. Justo, L. Távara, L. García-Guzmán, and F. París, “Characterization of 3D printed long fibre reinforced composites,” *Compos. Struct.*, vol. 185, no. October 2017, pp. 537–548, 2018, doi: 10.1016/j.compstruct.2017.11.052.

[32] W. Hao, Y. Liu, H. Zhou, H. Chen, and D. Fang, “Preparation and characterization of 3D printed continuous carbon fiber reinforced thermosetting composites,” *Polym. Test.*, vol. 65, no. September 2017, pp. 29–34, 2018, doi: 10.1016/j.polymertesting.2017.11.004.

[33] Y. Ming, S. Zhang, W. Han, B. Wang, Y. Duan, and H. Xiao, “Investigation on process parameters of 3D printed continuous carbon fiber-reinforced thermosetting epoxy composites,” *Addit. Manuf.*, vol. 33, no. March, p. 101184, 2020, doi: 10.1016/j.addma.2020.101184.

[34] W. Dong *et al.*, “Fabrication of a continuous carbon fiber-reinforced phenolic resin composites via in situ-curing 3D printing technology,” *Compos. Commun.*, vol. 38, no.

December 2022, p. 101497, 2023, doi: 10.1016/j.coco.2023.101497.

[35] “Epon-resin-8111-europe @ www.westlakeepoxy.com.” 2011. [Online]. Available: http://www.westlakeepoxy.com/en-US/product/epon-resin-8111---europe.

[36] “Technical data sheet Epikure 3271,” no. 1. pp. 430–439, 2018. [Online]. Available: https://www.westlakeepoxy.com/en-US/product/EPIKURE-Curing-Agent-3271.

[37] X. Huang, “Fabrication and properties of carbon fibers,” *Materials (Basel).*, vol. 2, no. 4, pp. 2369–2403, 2009, doi: 10.3390/ma2042369.

[38] ASTM D729, “Standard Test Methods for Density and Specific Gravity (Relative Density) of Plastics by Displacement,” *Am. Soc. Test. Mater.*, p. 6, 2008, doi: 10.1520/D0792-20.2.

[39] ASTM, “ D3039/D3039M,” *Annu. B. ASTM Stand.*, pp. 1–13, 2014, doi: 10.1520/D3039.

[40] E. I. Materials *et al.*, “Standard Test Method for Flexural Properties of Polymer Matrix Composite Materials 1,” pp. 1–11, 2012, doi: 10.1520/D7264.

[41] ASTM E1131 − 08, “Standard Test Method for Compositional Analysis by Thermogravimetry 1,” *ASTM Int.*, vol. 08, no. Reapproved 2014, p. 6, 2015, doi: 10.1520/E1131-20.2.

[42] "42GT-M24-8367-Lucifer-Oven.” [Online]. Available: https://luciferfurnaces.com/products/all-products/series-4000-gt-inert-atmosphere-gt-ovens/